PUCHI regulates very long chain fatty acid biosynthesis during lateral root and callus formation

Duy-Chi Trinh, Julien Lavenus, Tatsuaki Goh, Yohann Boutté, Quentin Drogue, Virginie Vaissayre, Frederique Tellier, Mikael Lucas, Ute Voss, Pascal Gantet, et al.

Classification: Biological Sciences, Plant Biology

Title

PUCHI regulates Very Long Chain Fatty Acid biosynthesis during lateral root and callus formation

Short title: PUCHI regulates VLCFA biosynthesis

Authors

Duy-Chi Trinh[a,b], Julien Lavenus[a,c], Tatsuaki Goh[d], Yohann Boutté[e], Quentin Drogue[a], Virginie Vaissayre[a], Frédérique Tellier[f], Mikaël Lucas[a], Ute Voß[c], Pascal Gantet[a], Jean-Denis Faure[f], Stéphane Dussert[a], Hidehiro Fukaki[g], Malcolm J. Bennett[c], Laurent Laplaze[a,*] and Soazig Guyomarc'h[a,*]

Affiliations

[a] UMR DIADE, Université de Montpellier, IRD, Montpellier, France

[b] Department of Pharmacological, Medical and Agronomical Biotechnology, University of Science and Technology of Hanoi, Hanoi, Vietnam

[c] University of Nottingham, Sutton Bonington, UK

[d] Graduate School of Science and Technology, Nara Institute of Science and Technology, Ikoma, Japan

[e] Laboratoire de Biogénèse Membranaire, UMR 5200, CNRS, Université de Bordeaux, Bordeaux, France

[f] Institut Jean-Pierre Bourgin, UMR 1318, INRA, AgroParisTech, CNRS, Université Paris-Saclay, Versailles, France

[g] Department of Biology, Graduate School of Science, Kobe University, Kobe, Japan

* To whom correspondence should be addressed. Laurent Laplaze and Soazig Guyomarc'h, IRD, UMR DIADE, 911 Avenue Agropolis, 34394 Montpellier cedex 5, France, laurent.laplaze@ird.fr and soazig.guyomarch@ird.fr; Tel: +33 4 67 41 64 62

Abstract

Lateral root organogenesis plays an essential role in elaborating plant root system architecture. In *Arabidopsis*, the AP2-family transcription factor PUCHI controls cell proliferation in lateral root primordia. To identify potential targets of PUCHI, we analyzed a time course transcriptomic dataset of lateral root formation. We report that multiple genes coding for very long chain fatty acid (VLCFA) biosynthesis enzymes are induced during lateral root development in a PUCHI-dependent manner. Significantly, several mutants perturbed in VLCFA biosynthesis show similar lateral root developmental defects as *puchi-1*. Moreover, *puchi-1* roots display the same disorganized callus formation phenotype as VLCFA biosynthesis deficient mutants when grown on auxin-rich callus inducing medium. Lipidomic profiling *puchi-1* roots revealed reduced VLCFA content compared to WT. We conclude that PUCHI-regulated VLCFA biosynthesis is part of a conserved pathway controlling cell proliferation during lateral root and callus formation.

137 words

lateral root formation | morphogenesis | VCLFA | callus formation | cell division

Significance

Lateral root organogenesis enables plant roots to branch and improve foraging for resources. Using a systems biology approach, we discovered expression of very long chain fatty acid (VLCFA) biosynthesis pathway genes are induced downstream of PUCHI, a transcription factor controlling cell division and morphogenesis during lateral root formation. Furthermore, we report that regulation of the VLCFA biosynthesis pathway by PUCHI is conserved for both lateral root development and callus formation, the first step in *in vitro* plant regeneration.

Author contributions

M.J.B., L.L., and S.G. designed research; T.D.C., J.L., T.G., Y.B., Q.D., V.V., F.T., U.V., S.D. performed research; T.D.C., J.L., T.G., Y.B., M.L., U.V., P.G., J.D.F., S.D., H.F., M.J.B., L.L., and S.G. analyzed data; and T.D.C., M.J.B., L.L. and S.G. wrote the paper.

\body

Introduction

Plant root system architecture (RSA) is the three-dimensional configuration of a whole root system in its living environment (1). RSA is considered a major determinant of plant viability and crop yield, and is a target for breeding to improve crop performance under various stresses (2, 3). Root branching is of particular importance because it largely determines the overall surface area of the root system and its spatial organization in the soil. Accordingly, the molecular mechanisms of root branching have been extensively studied in the model plant *Arabidopsis thaliana* whose mature root system is largely derived from lateral roots (LRs) formed after germination. LRs originate from a small group of xylem-pole pericycle cells of the primary root that are primed by auxin to acquire founder cell identity (4). These founder cells undergo a succession of anticlinal and periclinal cell divisions that eventually result in the formation of a dome-shaped lateral root primordium (LRP; 5–8). The LRP emerges through overlaying root tissues to become a LR (9, 10).

Lateral root development is an excellent experimental system to study *de novo* meristem formation (11). Moreover, recent studies have shown that lateral root formation shares common mechanisms with organ regeneration in tissue culture, especially the first step of callus formation (12–15). While many genes involved in lateral root development have been identified, little is known about the mechanisms that progressively organize the LRP into a new root meristem (16). LRP organization is not dependent on a stereotypical cell division pattern and therefore on cell lineage (6, 7). It is a dynamic process dependent on complex gene regulatory networks and on cell-cell interactions including hormonal and biomechanical signals (6, 10, 17). Interestingly, inference of the gene regulatory network involved in LR formation suggested an early patterning mechanism defining the central region and flanks of the LRP and identified genes involved in this process (18). One such gene encodes the AP2/EREBP-family transcription factor PUCHI which was previously shown to control cell proliferation during LRP formation (19). The *puchi-1* mutant LRP exhibits additional anticlinal and periclinal cell divisions from early stages and produces abnormally enlarged flank cells (19). PUCHI also controls LR density in combination with others transcription factors such as LBD16 and LBD18 (20). However, little is known about the pathways that are regulated by PUCHI.

VLCFA are fatty acids with 20 or more carbons synthesized in the endoplasmic reticulum from long chain-fatty acyl-CoA (16 or 18 carbons) by the fatty acid elongase complex (Fig. 1A). This complex catalyzes rounds of 2-carbon elongation in a 4-step mechanism, involving a 3-ketoacyl-CoA synthase (KCS), a 3-ketoacyl-CoA reductase (KCR), a 3-hydroxyacyl-CoA dehydratase (HACD), and a trans-2,3-enoyl-CoA reductase (ECR). Multiple KCS enzymes with various expression patterns have been described and their substrate affinity is thought to be responsible for the final VLCFA chain length (21–23). In contrast, only a limited number of genes that encode functional enzymes catalyzing each of the subsequent steps of the elongation cycle has been identified in Arabidopsis. *KETOACYL REDUCTASE 1* (*KCR1*) encodes an Arabidopsis KCR enzyme (24) while *PASTICCINO 2* (*PAS2;* 30) and *PROTEIN TYROSIN PHOSPHATASE-like* (*PTPLA*) encode two HACD enzymes (26). Last the product of the *ENOYL CO-A REDUCTASE/ECERIFERUM 10* (*ECR/CER10)* gene has ECR activity (27). These enzymes are physically linked together by PASTICCINO 1 (PAS1; Fig. 1A; 33). VLCFA are components of various classes of membrane, storage and extracellular lipids (29). VLCFA-containing sphingolipids and glycerolipids provide unique properties to membranes promoting inter-leaflet interactions and lipid rafts formation. As such, VLCFA influence membrane dynamics during cell division (30, 31), the distribution of membrane proteins such as auxin transporters (28, 32), and are involved in non cell-autonomous processes of growth regulation (33–35). In addition, VLCFA-containing lipids, or their derivatives, are thought to act as second messengers in response to various stimuli (36, 37). Finally, VLCFA are components of hydrophobic extracellular material *e.g.* in mammal skin barriers (38) or suberin and cuticular waxes in plants that protect tissues from uncontrolled water, gas and ion loss as well as from the invasion by environmental pathogens or contaminants (29).

In this study, we identified genes acting downstream of PUCHI using a time course LR transcriptomic dataset (39) combined with a gene regulatory network (GRN) inference algorithm (18). We found PUCHI-dependent expression of genes involved in the biosynthesis of very long chain fatty acids (VLCFA) during LR development. Consistently, VLCFA mutants display defects in LR development similar to *puchi-1*. VLCFA were previously described to regulate the competence of pericycle cells to generate calli on an auxin-rich callus-inducing medium (CIM) (21). We show that PUCHI is also expressed in CIM-treated roots and regulates the expression of genes involved in VLCFA biosynthesis during CIM-induced callus formation. Accordingly, CIM-

treated roots of the *puchi-1* mutant show reduced level of VLCFA as compared to wild type and exhibit comparable phenotype to VLCFA biosynthesis mutants. Our results indicate that PUCHI-regulated VLCFA biosynthesis is part of a conserved pathway controlling cell proliferation during LR and callus formation.

Results

PUCHI regulates VLCFA biosynthesis genes during lateral root development

To gain insight into the function(s) of PUCHI during LR development, we took advantage of the time-course transcriptomic dataset profiling every stage of LRP organogenesis (39) to identify candidate genes whose expression is regulated by this transcription factor. We employed the TDCor algorithm (18) to search the LR dataset for genes exhibiting an expression profile highly similar to that of *PUCHI* (Pearson's correlation coefficient > 0.80) when shifted back in time by 3 hours. Our *in silico* analysis retrieved 217 potential target genes whose expression profiles are correlated with that of *PUCHI* (*SI Appendix*, Table S1). A Gene Ontology (GO) enrichment analysis using BiNGO (40) revealed that 71 GO biological processes were significantly overrepresented in this group of putative downstream genes (*SI Appendix*, Table S2). Among them, the "VLCFA biosynthesis" category stood out as one of the most strongly overrepresented biological processes (p-value = 0.006). In the LR dataset, *PUCHI* transcript abundance rapidly rises after LR induction and peaks at around 12 hours after gravistimulation, which corresponds to the time when the first round of anticlinal cell division is observed (Fig. 1B, black line). *PUCHI* transcript levels then gradually decrease over time. Expression profiles of genes encoding key enzymes for each step of the VLCFA elongation cycle displayed comparable dynamics, albeit shifted in time. These included *KCS1, KCS2, KCS9, KCS17* and *KCS20* genes, all encoding members of the KCS enzyme family catalyzing the first step of VLCFA elongation, as well as *KCR1, PAS2* and *ECR/CER10*, which encode enzymes catalyzing the second, third, and fourth steps of VLCFA elongation, respectively, and *PAS1* (Fig. 1B and *SI Appendix*, Fig. S1).

We backed up this approach with a classical transcriptomic analysis of the *puchi-1* mutant complemented with a dexamethasone (DEX) inducible PUCHI-GLUCOCORTICOID RECEPTOR (GR) protein fusion expressed under the control of the *PUCHI* promoter. Treatment of *pPUCHI::PUCHI:GR/puchi-1* seedlings with DEX targets the recombinant transcription factor to the nucleus to regulate gene expression (41, 42) and restore the wild type (WT) LR phenotype

(Fig. S2). We used the auxin naphthaleneacetic acid (NAA) to induce LR formation and therefore increase the number of cells in which the PUCHI promoter is activated. Forty-six genes were significantly regulated (FC>1.5 and p-value<0.05) after 4h NAA + DEX treatment compared to NAA alone. Only 4 of these genes were common with the genes recovered from our previous analysis including 1 gene involved in VLCFA biosynthesis (*KCS8*) thus supporting activation of VLCFA biosynthesis genes downstream of PUCHI. However, this activation was lost when cycloheximide was added (Table S3). Hence, whilst expression of a set of genes encoding for the entire VLCFA elongation pathway was stimulated in a PUCHI-dependent manner during LR formation, these genes were not primary targets of PUCHI.

To confirm the PUCHI-dependent activation of the VLCFA biosynthesis pathway during LR development, we compared expression levels of VLCFA biosynthesis genes in WT and *puchi-1* roots during LR formation by RT-qPCR. An auxin-dependent LR induction system (LRIS, modified from 34; Fig. S3) was used to synchronously induce lateral root formation along the whole primary root. Transcript levels of *KCS1, KCS2, KCS20, KCR1, PAS2* and *ECR/CER10* were elevated after LR induction by NAA treatment in WT, but this response was disrupted in the *puchi-1* loss-of-function mutant background (Fig. 1C). Hence, genes encoding key components of the fatty acid elongase complex responsible for VLCFA biosynthesis are induced during LRP development, and this is dependent on the PUCHI transcription factor.

PUCHI controls the spatial expression of VLCFA synthesis genes during LR development

We next analyzed the spatial expression pattern of VLCFA synthesis genes during LR development using promoter-reporter gene fusions in WT and *puchi-1* backgrounds. A functional *pPUCHI::PUCHI:GFP* reporter is expressed throughout LRP during early stages of development, then the expression is excluded from the tip and limited to the flanks (Fig. 2A; 18). The functional *pKCS1::KCS1:GFP* reporter was expressed in the outermost layer of cells in LRP (Fig. 2B). We also monitored the expression pattern of promoter::GUS reporter fusions for *KCS6, KCS20, KCR1, PAS2* and *PAS1* genes in developing LRPs. In WT, *KCS6*, *KCR1*, *PAS2*, and *PAS1* reporter transgenes were strongly expressed in developing and emerging LRPs (Fig. 2C,E-G, whereas *pKCS20::GUS* was expressed in a few cells of LRPs (Fig. 2D). Interestingly, reporter transgenes displayed distinct expression patterns in emerging LRP, with *pKCS6::GUS, pKCS20::GUS* and *pPAS1::GUS* showing stronger activity at the base of emerging LRs (Fig. 2C,D,G) whereas

expression of *pKCS1::KCS1:GFP, pKCR1::GUS* and *pPAS2::GUS* was stronger at their tips (Fig. 2B,E,F).

When introgressed into the *puchi-1* background, we observed a clear reduction in *pKCS1::KCS1:GFP* and *pKCS6::GUS* expression, although mostly in developing LRPs (Fig. 2H,I). In contrast, *pKCS20::GUS* expression was clearly enhanced in *puchi-1* emerging LRs, especially at their tips (Fig. 2J). Loss of function of PUCHI also caused a clear and consistent decrease in expression of *pKCR1::GUS*, *pPAS2::GUS* and *pPAS1::GUS* in developing LRPs and emerging LRs (Fig. 2K-M). Interestingly, expression of these reporters became confined to several basal and flank cells in a majority of emerging LRs. In summary, our analyses confirmed that key VLCFA biosynthesis genes are expressed during LRP development and that their expression patterns in LRP are dependent on PUCHI.

PUCHI inhibits LR initiation but is necessary for later organ development

To better understand the role of PUCHI during LRP development, we carefully characterized the impact of the *puchi-1* mutation on LR formation. Emerged LRs and non-emerged LRPs were counted along the primary root of 9 day-old seedlings (Fig. 3A). LRPs located in the LR formation zone, *i.e.* rootwards of the most recently emerged LR, were scored as "developing LRPs" (Fig. 3A, 35). Although the density of emerged LRs was not significantly different between *puchi-1* and WT, the density of developing LRPs in the LR formation zone was almost three times higher in the mutant compared to WT (Fig. 3B). Consistent with this observation, the distances between two consecutive LRs were much shorter intervals in *puchi-1* than in WT (Fig. 3C). The distance between two adjacent LR organs in WT has been reported to be usually greater than 300µm (45). However, *puchi-1* roots frequently produced clusters of developing LRPs within 300µm of one another, either along a longitudinal (*i.e.* along a protoxylem pole) or radial (*i.e.* along opposite protoxylem poles) axis (Fig. 3C-D, 37). Thus, our data reveals that PUCHI represses LRP initiation in the pericycle and therefore controls the spacing between LRs.

In the root branching zone, *i.e.* shootward of the most recently emerged LR (Fig. 3A, 35), the density of emerged LRs was similar in the *puchi-1* and in the WT background, but a strikingly high number of non-emerged LRPs were also present in the mutant, consistent with the observation of higher LRP initiation rate in the LRP formation zone (Fig. 3B). These organs may correspond to arrested or delayed LRPs (45, 47, 48). To decipher between these two hypotheses, we marked

and counted the number of emerged LRP in the root branching zone first 9 days after germination and then again after 4 extra days of growth. In both WT and *puchi-1*, we observed that none or very few new LR had emerged during these additional days, consistent with the hypothesis that these unemerged LRPs have stopped developing (Table S4). Thus, our data suggest that in addition to LRP initiation density, loss of *PUCHI* function also impacts LRP development. To confirm this, we used a gravistimulation-based LR induction system (49, 50) to analyze the kinetics of LRP development in *puchi-1* compared to WT and scored the developmental stages reached by LRPs (5) 18 and 48 hours after induction (Fig. 3E). Gravistimulation induced the initiation of LRP development in almost 100% of the *puchi-1* and WT seedlings. However, a delay in *puchi-1* LRP development was already observed 18 hours post gravistimulation compared to WT. At 48 hours, a majority of WT LRP had emerged while most *puchi-1* LRP only reached developmental stages IV, V or VI (Fig. 3E). Furthermore, 6 days after gravistimulation, 100% (53/53) of induced LR had emerged in the WT background whereas only 70% (35/50) did so in the *puchi-1* background. Hence, PUCHI is required for normal developmental progression of LRPs and LR emergence.

VLCFA mutants display similar defects in lateral root development as *puchi-1*

We performed the same lateral root phenotyping assay for VLCFA mutants. We focused on mutants in *KCS* genes expressed downstream of PUCHI during lateral root development (*kcs1-5, kcs9, kcs2 kcs20*), and *ECR/CER10* genes because (i) mutants in *KCR1*, *PAS1* and *PAS2* display severe and pleiotropic developmental phenotypes (24, 25), (ii) loss-of-function phenotype for those *KCS*, and *ECR* genes have been described (23, 27, 28, 35, 51), and (iii) functional redundancy and substrate specificity of KCS enzymes have been studied (23, 52). We did not observe any significant differences in LRP formation and development between *kcs9* single mutants nor *kcs2 kcs20* double mutant and WT seedlings. However, *kcs1-5* mutant, a null allele for the *KCS1* gene (35), displayed a root branching phenotype similar to *puchi-1*, albeit milder, including an increase in LRP production, a higher number of non emerged LRPs in the root branching zone (Fig. 3B), a significant decrease in the distance between LRPs (Fig. 3C), and a delay in LRP development as revealed by gravistimulation assay (Fig. 3E). Mutants in *ECR* (*cer10-2*) produced similar but weaker phenotype with more lateral organs and an increased number of delayed LRPs as compared to WT (Fig. S4). Moreover, double *kcs1-5 kcs20* and *kcs1-5 cer10-2* mutants resulted in more pronounced LRP development defects compared to the corresponding single mutants (Fig. S5).

Hence, VLCFA biosynthesis loss-of-function mutants exhibited similar defects in LRP development as *puchi-1*. In both cases, defects were weaker than those observed in *puchi-1*, possibly due to the fact that PUCHI may simultaneously regulate multiple VLCFA genes and possibly other pathways, and that VLCFA enzymes may act redundantly as indicated by our double mutant analysis.

PUCHI and *VLCFAs* control pericycle cell proliferation on callus inducing medium

VLCFAs were recently shown to control the ability of pericycle cells to form calli in Arabidopsis roots (35). This prompted us to investigate the role of PUCHI during callus formation. We first analyzed *PUCHI* expression during CIM-induced callus formation. When seven-day old *pPUCHI::PUCHI:GFP* seedlings were incubated on CIM, reporter gene expression was observed in developing calli (Fig. 4A). We next tested the phenotype of the *puchi-1* mutant in response to CIM. Before being transferred to CIM, WT and *puchi-1* roots displayed comparable anatomy (Fig. 4B, upper panels). After 4 days on CIM, both WT and *puchi-1* roots responded to the hormonal treatment with pericycle cell proliferation (Fig. 4B, lower panels). However, whereas WT roots produced dome-shaped calli, the *puchi-1* mutant generated a continuous layer of dividing cells along its entire primary root. This phenotype was similar and stronger than the fused-calli phenotype displayed by the VLCFA biosynthesis deficient mutant *kcs1-5* (Fig. 4B; 22). DEX treatment restored a WT callus formation phenotype in *pPUCHI::PUCHI:GR*/*puchi-1* plants on CIM medium (Fig. 4C) thus confirming that the callus formation phenotype of *puchi-1* roots on CIM is caused by loss of function of *PUCHI*.

We next analyzed if PUCHI is required for the expression of VLCFA genes in the context of CIM-induced callus formation. *pKCS1::KCS1:GFP*, *pKCS6::GFP:GUS* and *pKCR1::GFP:GUS* expression were studied after CIM treatment in WT and *puchi-1* backgrounds. All three reporter genes were expressed in calli in WT plants and this expression was lost in *puchi-1* (Fig. S6). Hence, PUCHI and VLCFA restrict pericycle cell proliferation during callus formation and PUCHI is necessary for expression of VLCFA biosynthesis genes in response to CIM treatment.

***puchi-1* displays altered VLCFA content**

To further demonstrate that the *puchi-1* phenotypes were linked to changes in VLCFA content, we analyzed the fatty acid composition in WT, *kcs1-5* and *puchi-1* CIM-treated roots. CIM treatment

was chosen because of the strong associated phenotypes and as it generated a large amount of material for lipidomics. The total amount of fatty acids was similar in all 3 lines but the amount and proportion of VLCFAs was significantly lower in *kcs1-5* and *puchi-1* compared to WT (Fig. 4D&E). Interestingly, a detailed analysis of fatty acid-containing molecules showed that C22 fatty alcohols (22:0-OH) and C24 sphingolipids (h24:0) were significantly reduced in *puchi-1* while precursors (C18) were more abundant (Fig. S7). VLCFA are precursors of suberin and cutin biosynthesis. A suberin and cutin-like layer was recently described overlying developing LRP (Li et al Cur Biol 2017, Berhin et al Cell 2019). Suberin and root cutin are composed from dicarboxylic acid (DCA), ω-hydroxy acids (ωOH) and fatty alcohols (OH) (Delude et al., Plant Physiol 2016; Berhin et al., Cell 2019). Our lipid analyses indicate that neither DCA nor ωOH components are altered in *puchi* mutant as compared to WT (Fig. S7). We did not detect triOH-18:1, an atypical fatty acid enriched in root cap cuticle (Berhin et al., Cell 2019) but the level of all C18-containing fatty acids typical of suberin/cutin (ωOH-18, 18-DCA and 18-OH) was similar between *puchi* and WT (Fig. S7). However, we cannot exclude qualitative changes in composition of the suberin/cutin layer in front of LRP that would be regulated by PUCHI.

Discussion

We report that spatio-temporal expression of genes encoding VLCFA biosynthetic enzymes is coordinately regulated by PUCHI during LR formation. Interestingly, while expression of non-redundant *KCR1, PAS2* and *PAS1* genes (53, 54) is induced by PUCHI throughout developing LRPs in a similar manner, partially redundant *KCS* genes involved in the biosynthesis of VLCFAs of various chain lengths (23, 52, 54) displayed more diverse expression patterns and regulation. Our data suggest that VLCFAs of specific chain lengths may be synthesized and required in different cell types and/or at different stages of LRP development where they might contribute to LRP patterning.

The *puchi-1* loss-of-function mutant has been reported to exhibit LRPs with abnormal cell division patterns and with higher cell proliferation rates compared to WT at the organ flanks (19). We report a delay in LRP development and emergence, as well as higher initiation density along the primary root, with frequent clustering of primordia under both normal and tissue culture (CIM) conditions. This is consistent with previous studies indicating that VLCFAs are important to restrict cell proliferation (33). It was recently shown that VLCFA biosynthesis was also necessary

to organize cell proliferation into distinct calli in Arabidopsis roots grown on CIM (35). Importantly, callus formation shares common steps with the LRP formation pathway (13–15). We showed here that the *puchi-1* mutation causes roots to form a fused and continuous calli when treated with CIM, a phenotype reminiscent and even stronger than the one reported for *kcs1-5* and other mutants (35). Interestingly, roots of *puchi-1* and VLCFA mutants produced more LRPs than WT roots and these LRPs exhibit ectopic cell divisions, suggesting that PUCHI regulates a pathway restricting pericycle cell proliferation that is conserved between LR development and *in vitro* callus formation. Given that defects in VLCFA biosynthesis lead to cell over-proliferation in different contexts such as shoot vasculature (33, 55), CIM-induced calli (35; this study), and in LRPs (28), the regulation of VLCFA biosynthesis genes by PUCHI may explain at least in part the *puchi-1* LRP and CIM phenotype. PUCHI-regulated VLCFA biosynthesis might also be critical for cell patterning in lateral root primordia as evidenced by *puchi-1* phenotype and specific expression profiles of individual VLCFA biosynthesis genes. Further experiments will be needed to test this interesting hypothesis.

VLCFAs could regulate cell proliferation in several ways. VLCFAs can be incorporated into cell membranes and influence their structural and functional dynamics, especially endocytosis, vesicular trafficking, and exocytosis, impacting cell cytokinesis or the targeting to the membrane of important factors, such as auxin transporters (28, 32, 58). More generally, VLCFA content and composition may modulate hormonal signaling dynamics, especially cytokinins and auxins (33, 59). Last, VLCFA distribution could impact the mechanical properties of the tissues by modifying cell wall composition in the endodermis (24) or tissues that overlay LRPs (60).

Given the essential roles of VLCFAs during plant development, it is intriguing that *puchi-1* LRPs lacking the expression of key VLCFA biosynthesis genes such as *KCR1, PAS2* and *PAS1* were still be able to develop and emerge. This could be explained by partial redundancy or by non-cell-autonomous action of VLCFAs synthesized in other tissues or at earlier stages of development and in a PUCHI-independent way. Such non-cell-autonomous activity of VLCFAs has already been suggested in different contexts (33, 55, 61, 62).

In conclusion, using a systems biology approach we found that the expression of multiple important enzymes catalyzing each of the four steps of the VLCFA elongation cycle are upregulated during LRP development and this is dependent on the AP2/EREPB transcription

factor PUCHI. In addition, the *puchi-1* loss-of-function mutant shares similar LRP and callus phenotypes with mutants impaired in VLCFA biosynthesis. Hence, during root branching and root-derived callus formation the PUCHI transcription factor stimulates the expression of key VLCFAs biosynthesis genes in pericycle cells and their derivatives to regulate cell proliferation, organogenesis and organ spacing.

Methods

Plant materials and growth conditions

Arabidopsis thaliana seeds were sterilized and placed on squared Petri dishes containing ½ strength Murashige and Skoog (½ MS) solid medium containing 0.7% (w/v) plant agar supplemented with B5 vitamins. Plates were kept at 4ºC for 2 days and then placed in long-day conditions (16-h light/8-h dark cycle) in vertical position. The *puchi-1* and *pPUCHI::PUCHI:GFP/puchi-1* lines were previously described (19). The GUS reporter lines *pKCS6::GUS*, *pKCR1::GUS* and *pECR::GUS* were described in (21), *pKCS20::GUS* in (51), and *pPAS2::GUS* and *pPAS1::GUS* in (26). The *kcs1-5* mutant and *pKCS1::KCS1:GFP* line were described in (35), *kcs9* in (23) and *kcs2 kcs20* double mutant in (51).

To generate the PUCHI-GR plants, a genomic fragment of PUCHI, including the 3.9 kb promoter region and coding region, was amplified from genomic DNA using primers gPUCHI (5'-CACCCACGAGTGCAATCACACAGA-3') and gPUCHIrev-stop (5'-AAAGACTGAGTAGAAGCCTGTAGTGT-3') and subcloned into pENTR D-TOPO using Gateway technology. The genomic fragment was then transferred to pGWB-GR(C) that contains the Gateway cassette in front of the hormone-binding domain of rat glucocorticoid receptor (GR). The PUCHI-GR construct was transformed into the *puchi-1* mutant by floral dipping (63).

Bioinformatic analyses

To identify *PUCHI* potential targets based on correlation in expression profiles, an R script (Supporting information) was used in combination with the TDCor package (18) in R using the LR Dataset (39). GO enrichment analysis for biological processes was done using BiNGO plugin for Cytoscape (40, 64).

Gene expression analyses

Transcriptomic analysis of PUCHI-GR seedlings after induction by dexamethasone: 5-day old seedlings grown on 1x MS medium were transferred on the medium with or without the indicated chemicals (1 μM NAA, 2 μM DEX, and 10 μM CHX) for 4 hours. Total RNA was extracted from root tissue using the RNeasy Plant Mini Kit (Qiagen). Microarray analyses were performed with the Arabidopsis Genome ATH1 Array, and the experimental procedures were performed following the manufacturer's recommended protocols. All data were deposited in the Gene Expression

Omnibus (GEO) of the National Center for Biotechnology Information (NCBI) and are accessible through GEO accession number GSE128721. Transcriptome data were obtained from two biological replicates.

Targeted RT-qPCR analysis on puchi-1 and WT roots after LR induction by naphthaleneacetic acid: RT-qPCR analysis was performed on WT and *puchi-1* root materials prepared as previously described (43). Briefly, WT and *puchi-1* seeds were grown on ½ MS supplemented with 5µM naphthylphthalamic acid (NPA) for 14 days to inhibit lateral formation, then the seedlings were transferred to ½ MS supplemented with 5µM NPA or 10 µM naphthaleneacetic acid (NAA) to synchronously induce lateral root formation. Root materials were harvested after 24 hours (Fig. S3). *CYCLIN-DEPENDENT KINASE A;1* (*CDKA;1*; (65)) was used of normalization. The calibrator condition corresponds to NPA-treated WT roots. All of the RT-qPCR assays were performed with three biological replicates. Significance was determined by Student's t-test. Primers used are listed in *SI Appendix*, Table S5.

For GUS staining assay, 9-day old seedlings were incubated overnight at 37ºC in a phosphate buffer (pH 7) containing 5 mM potassium ferricyanide, 5 mM potassium ferrocyanide and 0.5 mg/mL 5-bromo-4-chloro-3-indolyl-beta-D-glucuronic acid (X-Gluc) dissolved in a small volume of dimethyl sulfoxide (DMSO). Samples were then washed by 70% ethanol, mounted on slides in a chloral hydrate:glycerol:water clearing solution (4:2:1 g/mL/mL) and visualized using DIC microscopy.

To visualize the expression of GFP reporter lines, seedlings were treated with 15µM propidium iodide (PI) supplemented with 0.004% Triton X-100 for 30-40 min as described in (66), and roots were observed under Leica TCS SP8 confocal microscope.

Root phenotyping

For lateral root density phenotyping, 9-day old, vertically grown seedlings were first imaged using a digital camera for root length measurement. Seedlings were then mounted in the chloral hydrate:glycerol:water clearing solution (4:2:1 g/mL/mL), and the number of developing LRPs, delayed LRPs and emerged LRs was counted. Primary root length was measured in Fiji using the SmartRoot plugin (67, 68).

For the gravistimulation assay, seedlings were first grown in squared Petri dishes at vertical position for 5 days, then dishes were turned by 90°. After 18 or 48 hours, seedlings were mounted in the chloral hydrate clearing solution; their LRPs were visualized under DIC microscopy and imaged. LRPs were categorized into developmental stages as described in (5).

For measurement of LR organ spacing distances, primary roots of 9-day old seedlings were progressively imaged from the collar to the tip under Zeiss AX10 DIC microscope at the magnification of 20x or 40x and pictures were manually stitched to produce a large view of the entire root. The distances between LR organs (including emerged LRs and non-emerged LRPs) were measured on this stitched image using Fiji (67).

Callus formation phenotyping

Callus formation assay was performed using the callus inducing medium (CIM) as described in (35). For *pPUCHI::PUCHI-GR*/*puchi-1* line, seedlings were cultured in ½ MS or CIM supplemented with 1 µM DEX.

Lipidomics profiling by GC-MS

Lipids were extracted as described in (69) and resuspended in 100 µl heptane:toluene (1:1, v/v). Samples were injected in a gas chromatography–mass spectrometry (GC-MS) chain composed of an analytic gaseous phase chromatograph (Agilent 7890 A) and a mass detector (MSD 5975 Agilent EI). Data were analyzed using the Agilent MassHunter Workstation software. Spectra were analyzed manually and confronted to the NIST mass spectral library to identify fatty acid compounds. Areas of peaks were normalized against corresponding standards to determine the quantity of each fatty acid.

Acknowledgements

We thank Dr. Martine Devic and Dr. Tom Roscoe (CNRS) for helpful discussions and critical reading of the manuscript. This work was supported by the Institute of Research for Development, the University of Montpellier, the University of Science and Technology of Hanoi and the French Embassy in Hanoi (Ph.D. grant to D.C.T.), the ENS Paris (PhD grant to J.L.) and the French National Research Agency (ANR) through the NewRoot project (ANR-17-CE13-0004-01 to M.L., L.L. and S.G.). U.V., and M.J.B. acknowledge the support of the Biotechnology and Biological

Sciences Research Council (BBSRC) and Engineering and Physical Sciences Research Council (EPSRC) funding to the Centre for Plant Integrative Biology (CPIB) BB/D019613/1 and from BBSRC grant BB/H020314/1. The IJPB benefits from support from the LabEx Saclay Plant Sciences-SPS (ANR-10-LABX-0040-SPS). Lipidomic analyses were performed on the Bordeaux Metabolome Facility-MetaboHUB (ANR-11-INBS-0010).

References

1. Morris EC, et al. (2017) Shaping 3D Root System Architecture. *Curr Biol* 27(17):R919–R930.
2. Smith S, De Smet I (2012) Root system architecture: insights from Arabidopsis and cereal crops. *Philos Trans R Soc B Biol Sci* 367(1595):1441–1452.
3. Zhan A, Schneider H, Lynch JP (2015) Reduced Lateral Root Branching Density Improves Drought Tolerance in Maize. *Plant Physiol* 168(4):1603–1615.
4. Möller BK, Xuan W, Beeckman T (2017) Dynamic control of lateral root positioning. *Curr Opin Plant Biol* 35:1–7.
5. Malamy JE, Benfey PN (1997) Organization and cell differentiation in lateral roots of Arabidopsis thaliana. *Development* 124(1):33–44.
6. Lucas M, et al. (2013) Lateral root morphogenesis is dependent on the mechanical properties of the overlaying tissues. *Proc Natl Acad Sci* 110(13):5229–5234.
7. Von Wangenheim D, et al. (2016) Rules and self-organizing properties of post-embryonic plant organ cell division patterns. *Curr Biol* 26(4):439–449.
8. Goh T, et al. (2016) Quiescent center initiation in the Arabidopsis lateral root primordia is dependent on the SCARECROW transcription factor. *Development* 143(18):3363–3371.
9. Swarup K, et al. (2008) The auxin influx carrier LAX3 promotes lateral root emergence. *Nat Cell Biol* 10(8):946–954.
10. Stoeckle D, Thellmann M, Vermeer JE (2018) Breakout — lateral root emergence in Arabidopsis thaliana. *Curr Opin Plant Biol* 41:67–72.
11. Lavenus J, Lucas M, Laplaze L, Guyomarc'h S (2013) The Dicot Root as a Model System for Studying Organogenesis. *Plant Organogenesis: Methods and Potocols, Methods in Molecular Biology*, pp 235–245.
12. Perianez-Rodriguez J, Manzano C, Moreno-Risueno MA (2014) Post-embryonic organogenesis and plant regeneration from tissues: two sides of the same coin? *Front Plant Sci* 5(May):1–11.
13. Fan M, Xu C, Xu K, Hu Y (2012) LATERAL ORGAN BOUNDARIES DOMAIN transcription factors direct callus formation in Arabidopsis regeneration. *Cell Res* 22(7):1169–1180.

14. Sugimoto K, Jiao Y, Meyerowitz EM (2010) Arabidopsis Regeneration from Multiple Tissues Occurs via a Root Development Pathway. *Dev Cell* 18(3):463–471.

15. Atta R, et al. (2009) Pluripotency of Arabidopsis xylem pericycle underlies shoot regeneration from root and hypocotyl explants grown in vitro. *Plant J* 57(4):626–644.

16. Trinh CD, Laplaze L, Guyomarc'h S (2018) Lateral Root Formation: Building a Meristem de novo. *Annual Plant Reviews Online* (John Wiley & Sons, Ltd, Chichester, UK), pp 1–44.

17. Du Y, Scheres B (2018) Lateral root formation and the multiple roles of auxin. *J Exp Bot* 69(2):155–167.

18. Lavenus J, et al. (2015) Inference of the Arabidopsis Lateral Root Gene Regulatory Network Suggests a Bifurcation Mechanism That Defines Primordia Flanking and Central Zones. *Plant Cell* 27(5):1368–1388.

19. Hirota A, Kato T, Fukaki H, Aida M, Tasaka M (2007) The auxin-regulated AP2/EREBP gene PUCHI is required for morphogenesis in the early lateral root primordium of Arabidopsis. *Plant Cell* 19(July):2156–2168.

20. Kang NY, Lee HW, Kim J (2013) The AP2/EREBP gene PUCHI co-acts with LBD16/ASL18 and LBD18/ASL20 downstream of ARF7 and ARF19 to regulate lateral root development in arabidopsis. *Plant Cell Physiol* 54(8):1326–1334.

21. Joubès J, et al. (2008) The VLCFA elongase gene family in Arabidopsis thaliana: Phylogenetic analysis, 3D modelling and expression profiling. *Plant Mol Biol* 67(5):547–566.

22. Millar AA, Kunst L (1997) Very-long-chain fatty acid biosynthesis is controlled through the expression and specificity of the condensing enzyme. *Plant J* 12(1):121–131.

23. Kim J, et al. (2013) Arabidopsis 3-Ketoacyl-Coenzyme A Synthase9 Is Involved in the Synthesis of Tetracosanoic Acids as Precursors of Cuticular Waxes, Suberins, Sphingolipids, and Phospholipids. *Plant Physiol* 162(2):567–580.

24. Beaudoin F, et al. (2009) Functional Characterization of the Arabidopsis -Ketoacyl-Coenzyme A Reductase Candidates of the Fatty Acid Elongase. *Plant Physiol* 150(3):1174–1191.

25. Bach L, et al. (2008) The very-long-chain hydroxy fatty acyl-CoA dehydratase PASTICCINO2 is essential and limiting for plant development. *Proc Natl Acad Sci* 105(38):14727–14731.

26. Morineau C, et al. (2016) Dual fatty acid elongase complex interactions in arabidopsis. *PLoS One* 11(9):1–20.

27. Zheng H (2005) Disruptions of the Arabidopsis Enoyl-CoA Reductase Gene Reveal an Essential Role for Very-Long-Chain Fatty Acid Synthesis in Cell Expansion during Plant Morphogenesis. *Plant Cell Online* 17(5):1467–1481.

28. Roudier F, et al. (2010) Very-Long-Chain Fatty Acids Are Involved in Polar Auxin

Transport and Developmental Patterning in Arabidopsis. *Plant Cell* 22(2):364–375.

29. Li-Beisson Y, et al. (2013) Acyl-Lipid Metabolism. *Arab B* 11:e0161.

30. Bach L, et al. (2011) Very-long-chain fatty acids are required for cell plate formation during cytokinesis in Arabidopsis thaliana. *J Cell Sci* 124(19):3223–3234.

31. Molino D, et al. (2014) Inhibition of very long acyl chain sphingolipid synthesis modifies membrane dynamics during plant cytokinesis. *Biochim Biophys Acta - Mol Cell Biol Lipids* 1841(10):1422–1430.

32. Wattelet-Boyer V, et al. (2016) Enrichment of hydroxylated C24-and C26-acyl-chain sphingolipids mediates PIN2 apical sorting at trans-Golgi network subdomains. *Nat Commun* 7. doi:10.1038/ncomms12788.

33. Nobusawa T, et al. (2013) Synthesis of Very-Long-Chain Fatty Acids in the Epidermis Controls Plant Organ Growth by Restricting Cell Proliferation. *PLoS Biol* 11(4):e1001531.

34. Yamauchi T, et al. (2015) Ethylene Biosynthesis Is Promoted by Very-Long-Chain Fatty Acids during Lysigenous Aerenchyma Formation in Rice Roots. *Plant Physiol* 169(1):180–193.

35. Shang B, et al. (2016) Very-long-chain fatty acids restrict regeneration capacity by confining pericycle competence for callus formation in *Arabidopsis*. *Proc Natl Acad Sci* 113(18):5101–5106.

36. Poulos A (1995) Very long chain fatty acids in higher animals-A review. *Lipids* 30(1):1–14.

37. De Bigault Du Granrut A, Cacas J-L (2016) How Very-Long-Chain Fatty Acids Could Signal Stressful Conditions in Plants? *Front Plant Sci* 7(October):1–13.

38. Kihara A (2012) Very long-chain fatty acids: Elongation, physiology and related disorders. *J Biochem* 152(5):387–395.

39. Voß U, et al. (2015) The circadian clock rephases during lateral root organ initiation in Arabidopsis thaliana. *Nat Commun* 6(May). doi:10.1038/ncomms8641.

40. Maere S, Heymans K, Kuiper M (2005) BiNGO: A Cytoscape plugin to assess overrepresentation of Gene Ontology categories in Biological Networks. *Bioinformatics* 21(16):3448–3449.

41. Schena M, Lloyd a M, Davis RW (1991) A steroid-inducible gene expression system for plant cells. *Proc Natl Acad Sci U S A* 88(23):10421–10425.

42. Aoyama T, Chua NH (1997) A glucocorticoid-mediated transcriptional induction system in transgenic plants. *Plant J* 11:605–612.

43. Himanen K, et al. (2004) Transcript profiling of early lateral root initiation. *Proc Natl Acad Sci U S A* 101(14):5146–5151.

44. Dubrovsky JG, Forde BG (2012) Quantitative Analysis of Lateral Root Development:

Pitfalls and How to Avoid Them. *Plant Cell* 24(1):4–14.

45. Dubrovsky JG, Gambetta GA, Hernández-Barrera A, Shishkova S, González I (2006) Lateral root initiation in Arabidopsis: Developmental window, spatial patterning, density and predictability. *Ann Bot* 97(5):903–915.

46. Hofhuis H, et al. (2013) Phyllotaxis and rhizotaxis in Arabidopsis are modified by three plethora transcription factors. *Curr Biol* 23(11):956–962.

47. Celenza JL, Grisafi PL, Fink GR (1995) A pathway for lateral root formation in Arabidopsis thaliana. *Genes Dev* 9(17):2131–42.

48. Nacry P, et al. (2005) A role for auxin redistribution in the responses of the root system architecture to phosphate starvation in Arabidopsis. *Plant Physiol* 138(4):2061–74.

49. Lucas M, Godin C, Jay-Allemand C, Laplaze L (2008) Auxin fluxes in the root apex co-regulate gravitropism and lateral root initiation. *J Exp Bot* 59(1):55–66.

50. Péret B, et al. (2012) Auxin regulates aquaporin function to facilitate lateral root emergence. *Nat Cell Biol* 14(10):991–998.

51. Lee SB, et al. (2009) Two Arabidopsis 3-ketoacyl CoA synthase genes, KCS20 and KCS2/DAISY, are functionally redundant in cuticular wax and root suberin biosynthesis, but differentially controlled by osmotic stress. *Plant J* 60(3):462–475.

52. Kosma DK, et al. (2014) AtMYB41 activates ectopic suberin synthesis and assembly in multiple plant species and cell types. *Plant J* 80(2):216–229.

53. Bach L, Faure JD (2010) Role of very-long-chain fatty acids in plant development, when chain length does matter. *Comptes Rendus - Biol* 333(4):361–370.

54. Haslam TM, Kunst L (2013) Extending The Story Of Very-Long-Chain Fatty Acid Elongation. *Plant Sci* 210:93–107.

55. Bellec Y, et al. (2002) Pasticcino2 is a protein tyrosine phosphatase-like involved in cell proliferation and differentiation in Arabidopsis. *Plant J* 32(5):713–722.

56. Hirota A, Kato T, Fukaki H, Aida M, Tasaka M (2007) The Auxin-Regulated AP2/EREBP Gene PUCHI Is Required for Morphogenesis in the Early Lateral Root Primordium of Arabidopsis. *Plant Cell Online* 19(7):2156–2168.

57. Park CS, Go YS, Suh MC (2016) Cuticular wax biosynthesis is positively regulated by WRINKLED4, an AP2/ERF-type transcription factor, in Arabidopsis stems. *Plant J* 88(2):257–270.

58. Bach L, et al. (2011) Very-long-chain fatty acids are required for cell plate formation during cytokinesis in Arabidopsis thaliana. *J Cell Sci* 124(Pt 19):3223–34.

59. Harrar Y, Bellec Y, Bellini C, Faure J (2003) Hormonal control of cell proliferation requires PASTICCINO genes. *Plant Physiol* 132(3):1217–1227.

60. Li B, et al. (2017) Role of LOTR1 in Nutrient Transport through Organization of Spatial Distribution of Root Endodermal Barriers. *Curr Biol* 27(5):758–765.

61. Faure JD, et al. (1998) The PASTICCINO genes of Arabidopsis thaliana are involved in the control of cell division and differentiation. *Development* 125(5):909–918.

62. Haberer G, Erschadi S, Torres-Ruiz RA (2002) The Arabidopsis gene PEPINO/PASTICCINO2 is required for proliferation control of meristematic and non-meristematic cells and encodes a putative anti-phosphatase. *Dev Genes Evol* 212(11):542–550.

63. Clough SJ, Bent AF (1998) Floral dip: A simplified method for Agrobacterium-mediated transformation of Arabidopsis thaliana. *Plant J* 16(6):735–743.

64. Shannon P (2003) Cytoscape: A Software Environment for Integrated Models of Biomolecular Interaction Networks. *Genome Res* 13(11):2498–2504.

65. Iwakawa H, Shinmyo A, Sekine M (2006) Arabidopsis CDKA;1, a cdc2 homologue, controls proliferation of generative cells in male gametogenesis. *Plant J* 45(5):819–831.

66. Du Y, Scheres B (2017) PLETHORA transcription factors orchestrate de novo organ patterning during *Arabidopsis* lateral root outgrowth. *Proc Natl Acad Sci* 114(44):201714410.

67. Schindelin J, et al. (2012) Fiji: An open-source platform for biological-image analysis. *Nat Methods* 9(7):676–682.

68. Lobet G, Pagès L, Draye X (2011) A Novel Image-Analysis Toolbox Enabling Quantitative Analysis of Root System Architecture. *Plant Physiol* 157(1):29–39.

69. Delude C, et al. (2016) Primary Fatty Alcohols Are Major Components of Suberized Root Tissues of Arabidopsis in the Form of Alkyl Hydroxycinnamates. *Plant Physiol* 171(3):1934–1950.

Figure Legends

Figure 1. Expression levels of key VLCFA biosynthesis genes are induced during LRP development in a PUCHI-dependent manner. (A) Schematic representation of the VLCFA elongation cycle. VLCFAs are synthesized from malonyl-CoA and acyl-CoA (number of carbon atoms in the chain n ≥ 16) by the fatty acid elongase complex comprised of KCS, KCR, HACD (PAS2) and ECR enzymes. PAS1 acts as a scaffold for the complex. (B) Expression profiles of *PUCHI* and selected VLCFA biosynthesis genes extracted from the lateral root development dataset (39). Transcripts accumulation levels are expressed in arbitrary units (A.U.). The gray dotted line indicates the time point when *PUCHI* expression reaches a maximum after LR induction. Note the similarity between the expression profiles and the delay between PUCHI expression peak and that of its putative target genes. (C) Measurement of key VLCFA biosynthetic gene expression by RT-qPCR in WT (blue) and *puchi-1* roots (orange). Lateral root formation is inhibited in control plants treated with NPA (darker shade), while on NAA (brighter shade) lateral root initiation is induced synchronously along the primary root in both WT and *puchi-1*. Roots were harvested after 24h treatment on 5 µM NPA or 10 µM NAA. Normalization was achieved with the *CYCLIN-DEPENDENT KINASE A;1* (*CDKA;1*) gene. The calibrator cDNA is WT under NPA treatment. Data are represented as Mean ± SEM (standard error of the means) of three biological replicates. Significance was determined by Student's t test (* $P < 0.05$, ** $P < 0.01$).

Fig. 2: VLCFA genes are expressed in developing LRPs and their expression patterns are dependent on PUCHI. (A) Expression of *pPUCHI::PUCHI-GFP* in *puchi-1* background is observed in developing LRP and is gradually confined to their base and flanks. (B) to (M) Expression patterns of various translational and transcriptional reporter constructs of VLCFA biosynthesis genes in typical WT (B to G) and *puchi-1* (H to M) LRPs and newly emerged LRs. A clear loss of GUS staining is observed in the case of *pKSC1::KCS1:GFP, pKCS6::GUS, pKCR1::GUS*, *pPAS2::GUS* and *pPAS1::GUS* in developing *puchi-1* LRPs compare to WT. Scale bars = 50µm. Numbers indicate the percentage of LRPs or LRs displaying the corresponding expression pattern. n = 30-40 seedlings for each GUS assay.

Figure 3. In *puchi-1* mutant LRP initiation is enhanced but their development is delayed. (A) Root branching events were scored in three distinct developmental zones of Arabidopsis primary root regarding lateral root formation as suggested in (44). (B) Density of developing LRPs, emerged LRs, delayed LRPs, and total LR initiations (LRPs + LRs) in 9-day old WT, *puchi-1* and *kcs1-5* seedlings. Developing LRPs are LRPs scored in the LR formation zone. Delayed LRPs are defined as those located in the branching zone of the primary root but have not crossed the epidermis. Data are represented as Mean ± SEM of three biological replicates; number of seedlings ≥ 20 in each repeat. Significance was determined by Student's t test. (C) Frequency distribution of distances between two consecutive LRPs in WT, *kcs1-5* and *puchi-1* roots. Each bin of the histogram

represents a range of 300 µm. Number of LRPs = 222, 208 and 228 for WT, *kcs1-5* and *puchi-1*, respectively. The orange bar in each histogram indicates the mean LRP distance in each genotype. The stars in the histograms for *kcs1-5* and *puchi-1* indicate the significant difference between these mean distances compared to that of WT. (D) Examples of longitudinal and radial clusters of LRPs in *puchi-1* roots. Arrowheads indicate LRPs. Scale bars = 50µm. (E) Distribution of developmental stages as described by Malamy and Benfey (5) achieved by gravistimulation-induced LRP formation in WT, *kcs1-5* and *puchi-1* roots at 18 and 48 hours after the gravistimulation. Data are represented as Mean ± SEM of three biological replicates, with number of seedlings ≥ 20 in each repeat. For all occasions, * $P < 0.05$, ** $P < 0.01$, *** $P < 0.001$.

Figure 4: Callus formation is enhanced in *puchi-1* roots. (A) *pPUCHI::PUCHI-GFP* (*PUCHI-GFP* for short) is expressed in calli induced by CIM, scale bars = 50 µm. (B) While *puchi-1, kcs1-5* and WT roots of 7-day-old seedlings display similar radial organization when grown on ½ MS medium (top), 4 more days of growth on CIM induces the formation of dome-shaped individual calli in WT, but of a continuous layer of proliferating cells in the *puchi-1* and *kcs1-5* background (bottom). (C) *pPUCHI::PUCHI-GR*/*puchi-1* plus dexamethasone (DEX) restores callus formation in *puchi-1* roots on CIM. n = 40 for WT, *kcs1-5* and *puchi-1*. n = 20 for *pPUCHI::PUCHI-GR*/*puchi-1*, scale bars = 0.1mm. (D) Quantification of fatty acids by GC-MS in WT, *puchi-1* and *kcs1-5* roots after 4 days on CIM. Both mutation results in a significant reduction in the proportion of VLCFAs (C≥20) over the total amount of fatty acids. (E) Global fatty acids of WT, *puchi-1* and *kcs1-5* roots after 4 days on CIM. The results are the sum of carboxylic acids, α,ω-dicarboxylic acids, ω-hydroxy acids, fatty alcohols and 2-hydroxy fatty acids. Both mutation results in a reduction of the amount of C22:0 and C24:0 and an increase in the C≤18 fatty acids, precursors of VLCFAs. The loss of KCS1 function also impacts C20:0 amounts, while the loss of function of PUCHI leads to a decrease in C26:0 content. Data are represented as Mean ± SEM of six, six and five biological replicates for WT, *puchi-1* and *kcs1-5*, respectively. * $P < 0.05$, ** $P < 0.01$, *** $P < 0.001$. * $P < 0.05$, ** $P < 0.01$, *** $P < 0.001$.

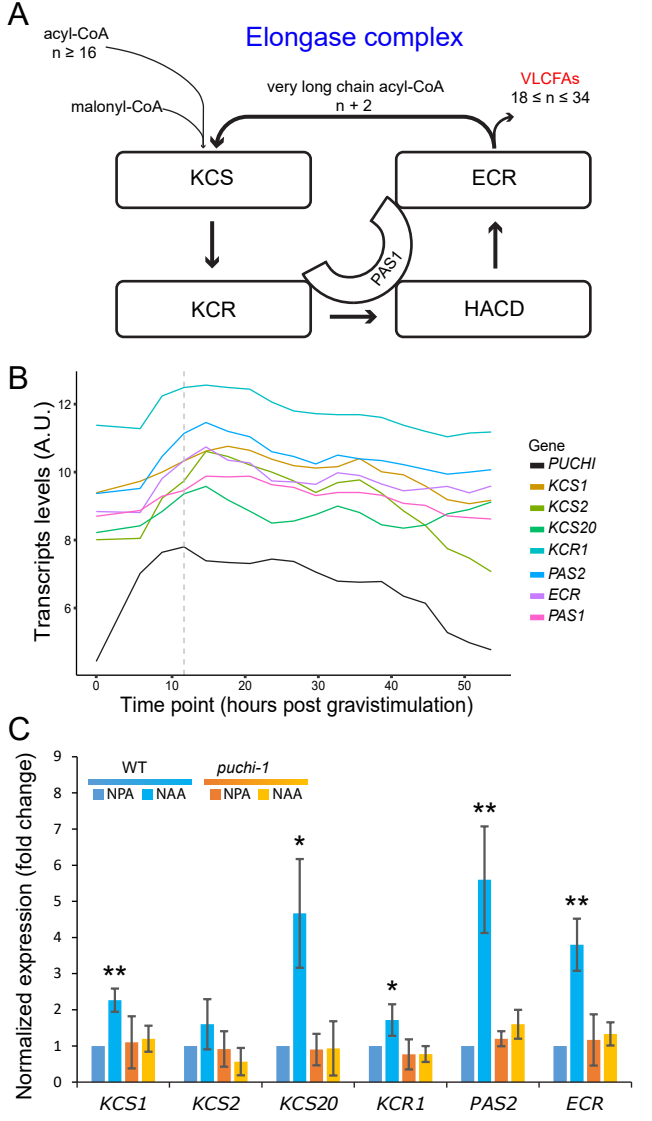
A
Elongase complex
acyl-CoA
n ≥ 16
malonyl-CoA
very long chain acyl-CoA
n + 2
VLCFAs
18 ≤ n ≤ 34
KCS
ECR
PAS1
KCR
HACD
B
Transcripts levels (A.U.)
Time point (hours post gravistimulation)
Gene
PUCHI
KCS1
KCS2
KCS20
KCR1
PAS2
ECR
PAS1
C
Normalized expression (fold change)
WT
puchi-1
NPA
NAA
NPA
NAA
KCS1
KCS2
KCS20
KCR1
PAS2
ECR

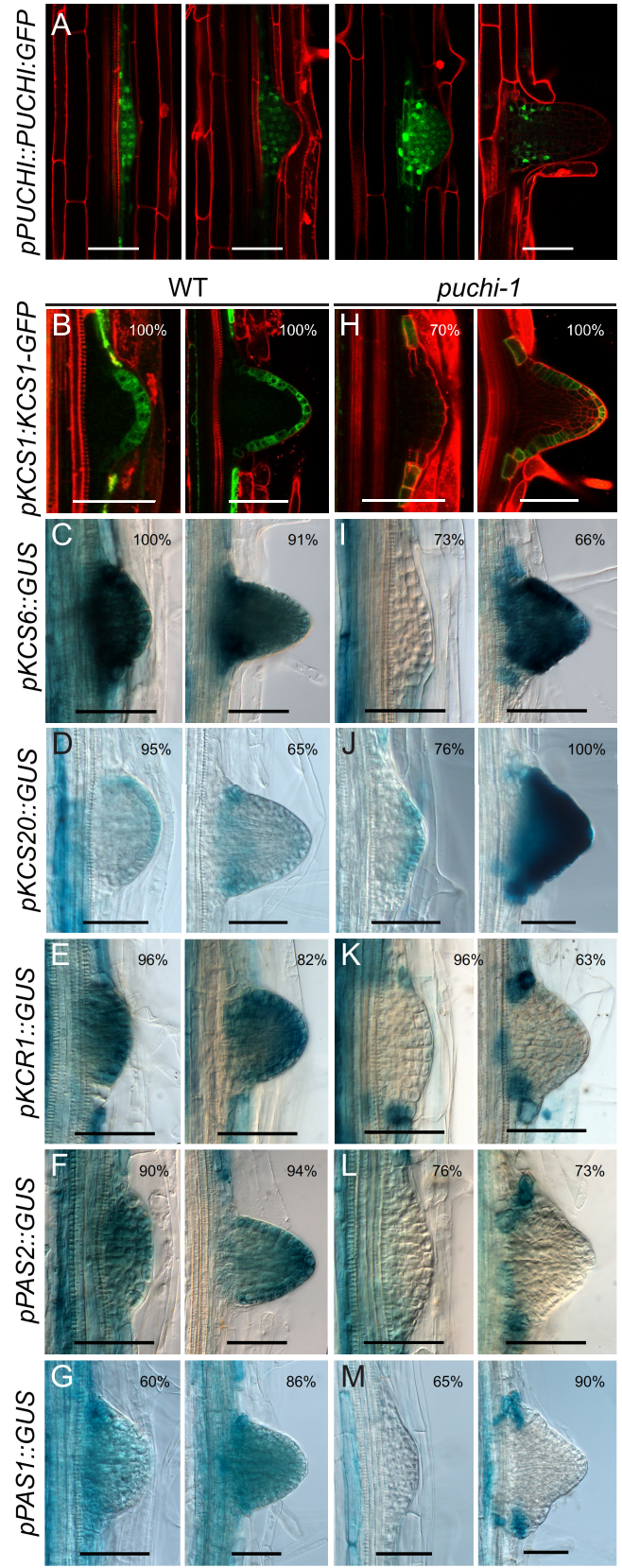
A
pPUCHI::PUCHI:GFP
WT
puchi-1
B
100%
100%
H
70%
100%
pKCS1:KCS1-GFP
C
100%
91%
I
73%
66%
pKCS6::GUS
D
95%
65%
J
76%
100%
pKCS20::GUS
E
96%
82%
K
96%
63%
pKCR1::GUS
F
90%
94%
L
76%
73%
pPAS2::GUS
G
60%
86%
M
65%
90%
pPAS1::GUS

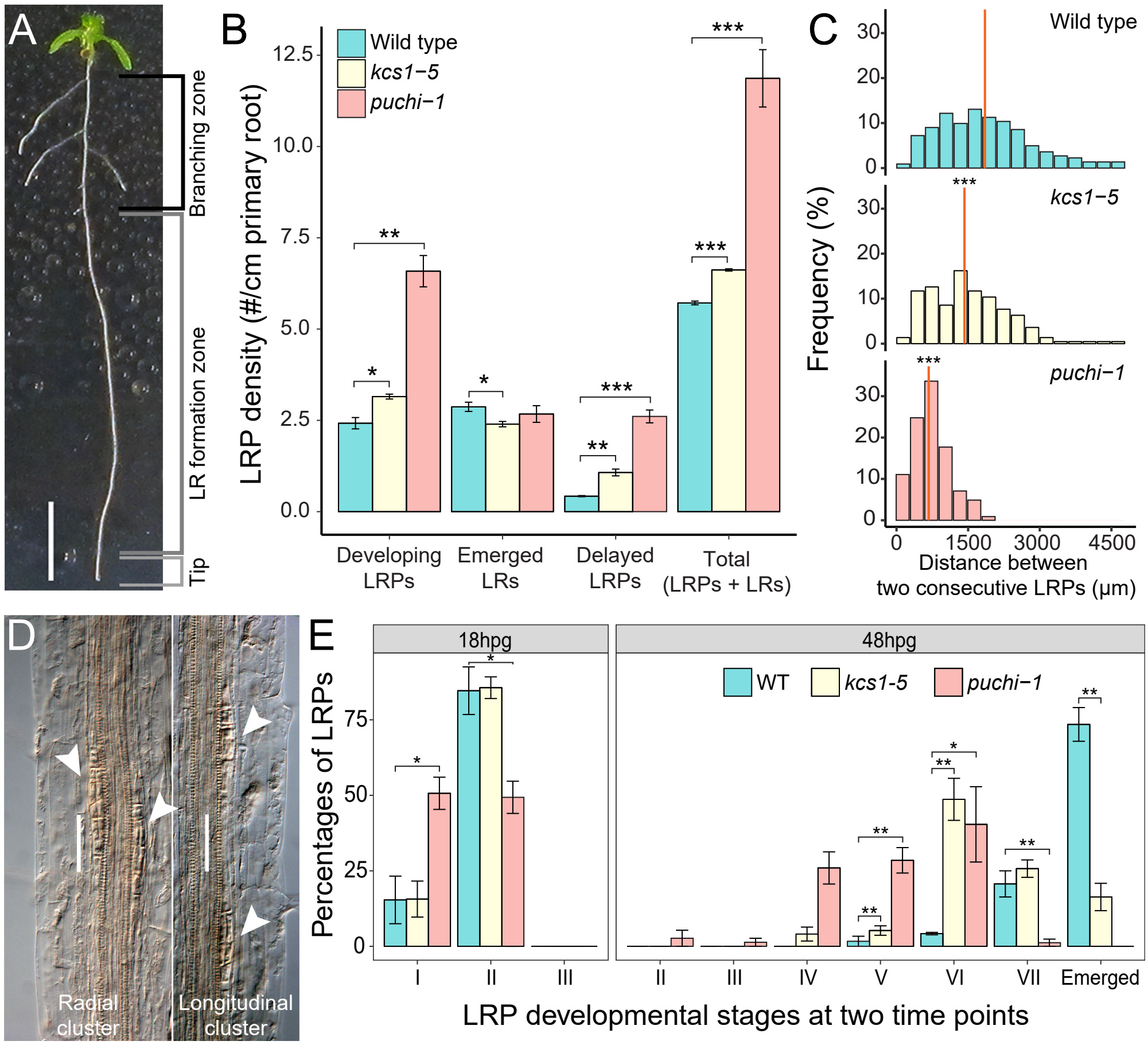
A
Branching zone
LR formation zone
Tip
B
Wild type
kcs1−5
puchi−1
LRP density (#/cm primary root)
12.5
10.0
7.5
5.0
2.5
0.0
Developing LRPs
Emerged LRs
Delayed LRPs
Total (LRPs + LRs)
C
Wild type
kcs1−5
puchi−1
Frequency (%)
Distance between two consecutive LRPs (μm)
D
Radial cluster
Longitudinal cluster
E
18hpg
48hpg
WT
kcs1-5
puchi−1
Percentages of LRPs
LRP developmental stages at two time points
Emerged

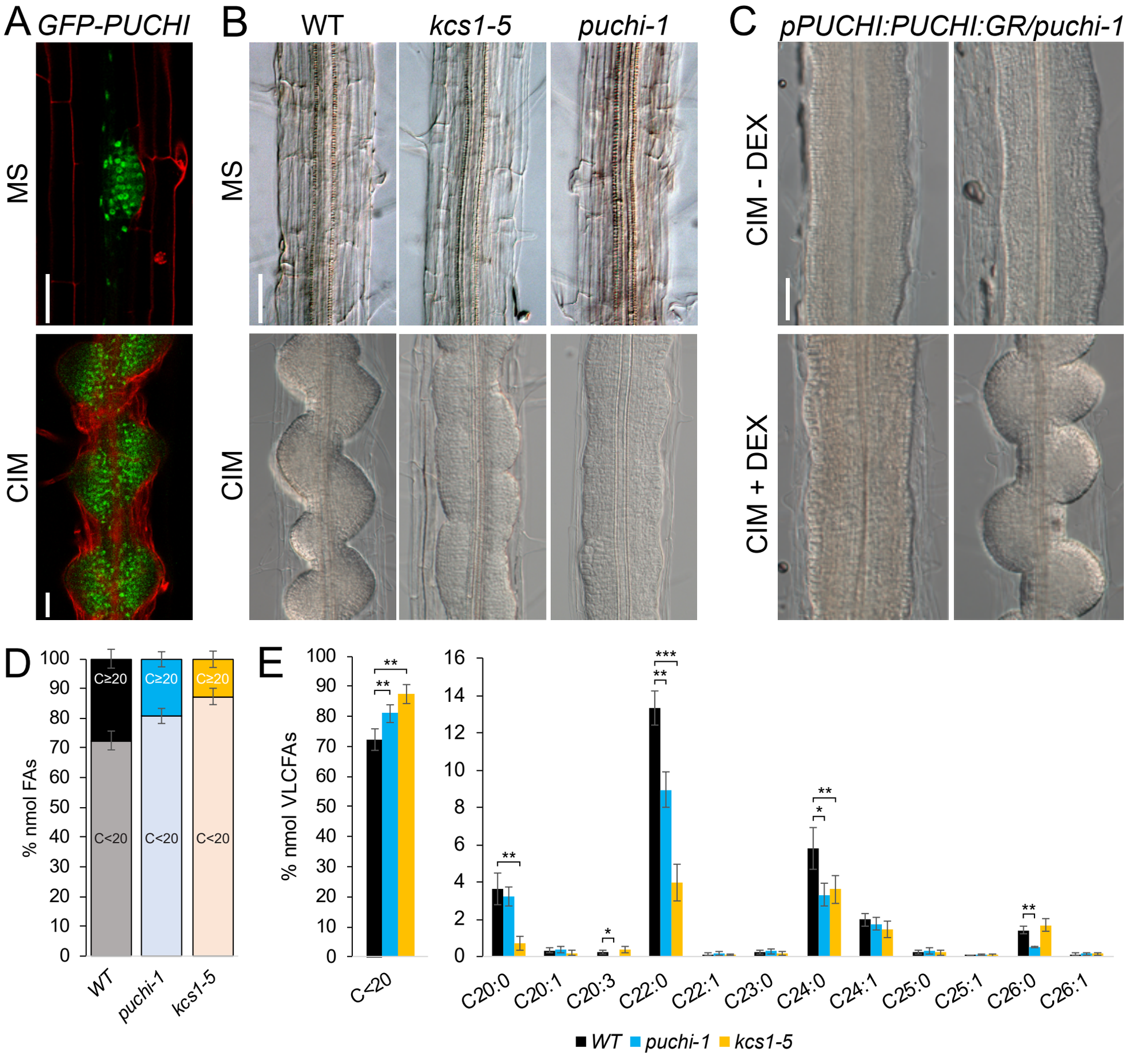
A
GFP-PUCHI
MS
CIM
B
WT
kcs1-5
puchi-1
MS
CIM
C
pPUCHI:PUCHI:GR/puchi-1
CIM - DEX
CIM + DEX
D
% nmol FAs
C≥20
C<20
WT
puchi-1
kcs1-5
E
% nmol VLCFAs
C<20
C20:0
C20:1
C20:3
C22:0
C22:1
C23:0
C24:0
C24:1
C25:0
C25:1
C26:0
C26:1
WT
puchi-1
kcs1-5

PNAS
www.pnas.org

Supplementary Information for

PUCHI regulates Very Long Chain Fatty Acid biosynthesis during lateral root and callus formation

Duy-Chi Trinh[a,b], Julien Lavenus[a,c], Tatsuaki Goh[d], Yohann Boutté[e], Quentin Drogue[a], Virginie Vaissayre[a], Frédérique Tellier[f], Mikaël Lucas[a], Ute Voß[c], Pascal Gantet[a], Jean-Denis Faure[f], Stéphane Dussert[a], Hidehiro Fukaki[g], Malcolm J. Bennett[c], Laurent Laplaze[a,*] and Soazig Guyomarc'h[a,*]

Corresponding author
Laurent Laplaze and Soazig Guyomarc'h, IRD, UMR DIADE, 911 Avenue Agropolis, 34394 Montpellier cedex 5, France. Email: laurent.laplaze@ird.fr, soazig.guyomarch@ird.fr.

This PDF file includes:

Supplementary Information Text

Methods

Identification of potential targets of PUCHI

To identify *PUCHI* potential targets based on correlation in expression profiles, the following script was used with the TDCor package (1) in R:

```
## To search for genes having correlated profiles
load("Path/TDCOREG 5.3.Rdata")
# correlation with time delay
k= as.vector(cor.data(rd[,2:18],rd["AT5G18560",1:17])) # AT5G18560:
PUCHI
names(k)=rownames(rd)
k[k>0.8]
write.table(names(k)[k>0.8],"AT5G18560 _cor_80_delay.txt")
# found 217 genes in the table
```

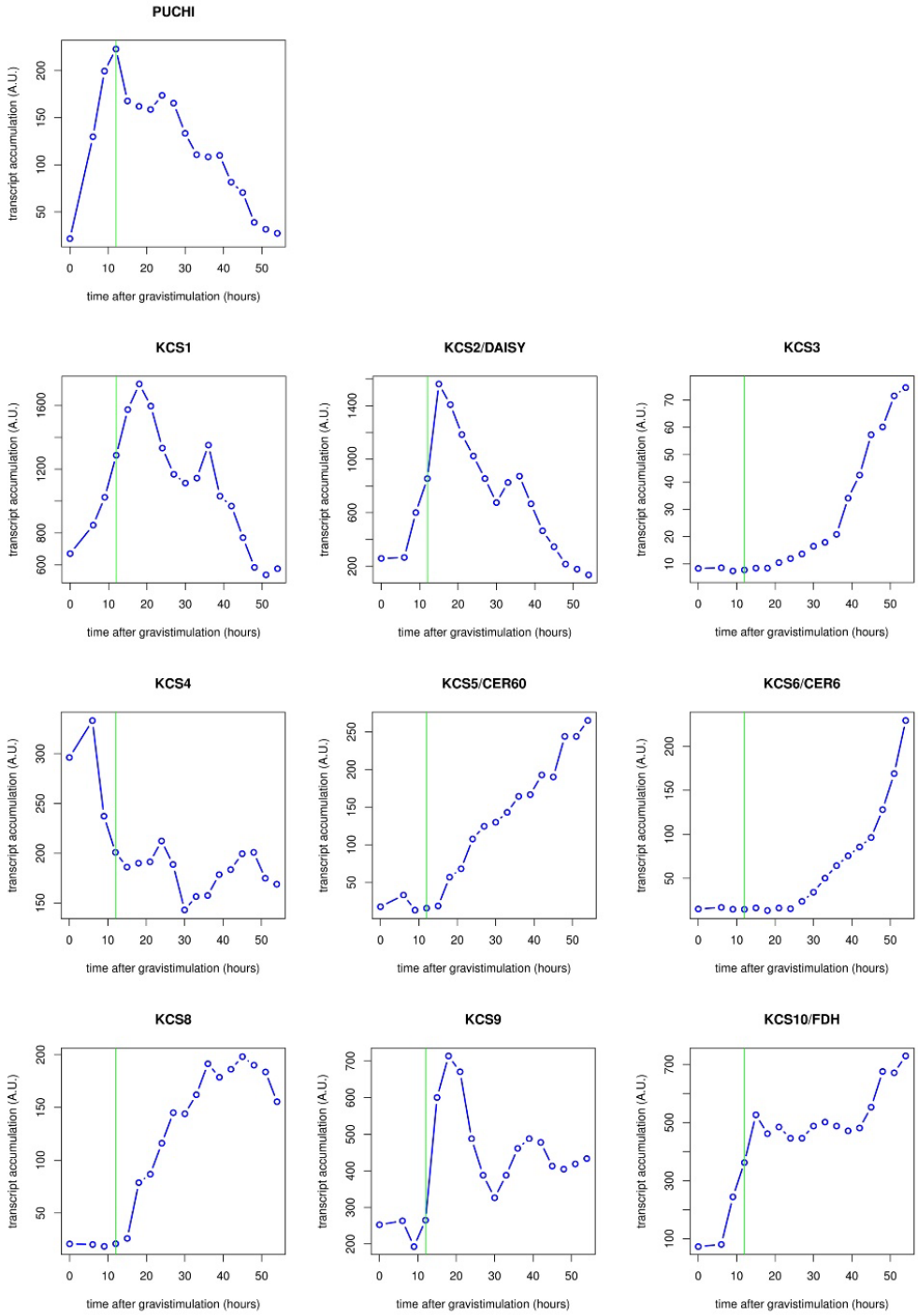

Fig. S1. Expression profiles of PUCHI and all known genes encoding for enzymes in the fatty acid elongase complex retrieved from the transcriptomic dataset (2). Transcripts accumulation levels are expressed in arbitrary units (A.U.). The green line indicates the time point when PUCHI expression reaches a maximum.

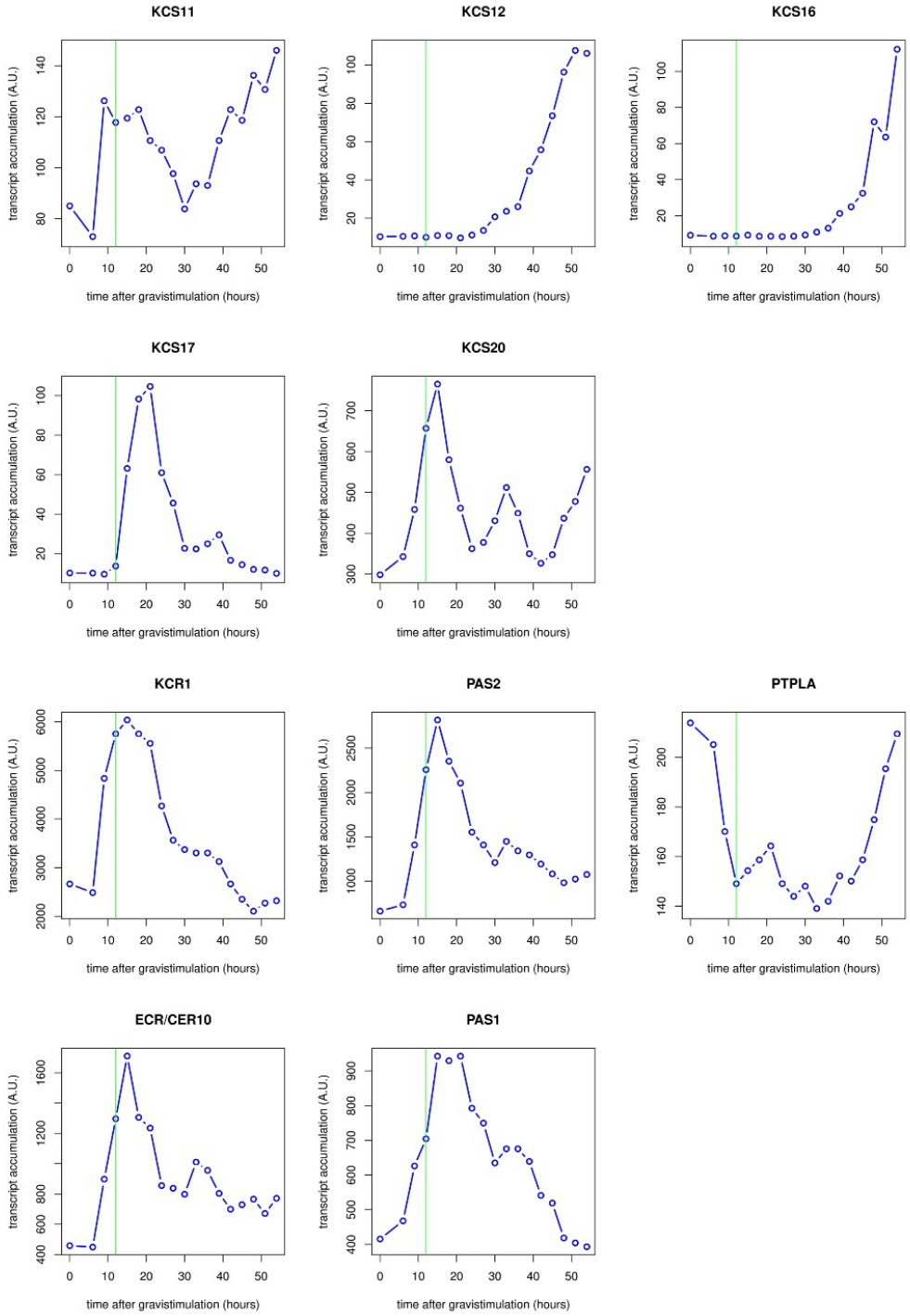

Fig. S1. (continued) Expression profiles of PUCHI and all known genes encoding for enzymes in the fatty acid elongase complex retrieved from the transcriptomic dataset (2). Transcripts accumulation levels are expressed in arbitrary units (A.U.). The green line indicates the time point when PUCHI expression reaches a maximum.

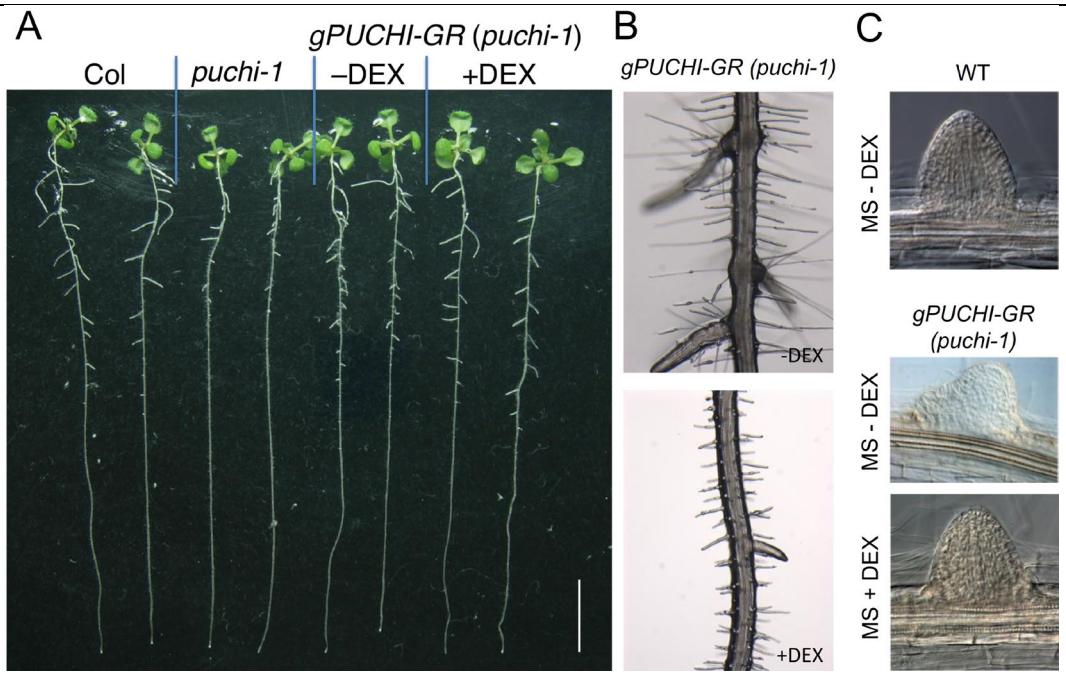

Fig. S2. Treatment of *pPUCHI::PUCHI:GR* in *puchi-1* background (*gPUCHI-GR (puchi-1)*) seedlings with dexamethasone (DEX) rescued *puchi-1* LR phenotype. (A) Whole plants (2 for each genotype) showing that *puchi-1* and *pPUCHI::PUCHI:GR (puchi-1)* without DEX produced more and closely-spaced LRs compared to the WT, while *pPUCHI::PUCHI:GR (puchi-1)* seedlings treated with DEX had WT-like LR production. (B) A closer view of LRs in *gPUCHI-GR (puchi-1)* seedlings treated with or without DEX. (C) DEX treatment of *gPUCHI-GR (puchi-1)* seedlings rescued the defective LRP morphology in *puchi-1* background.

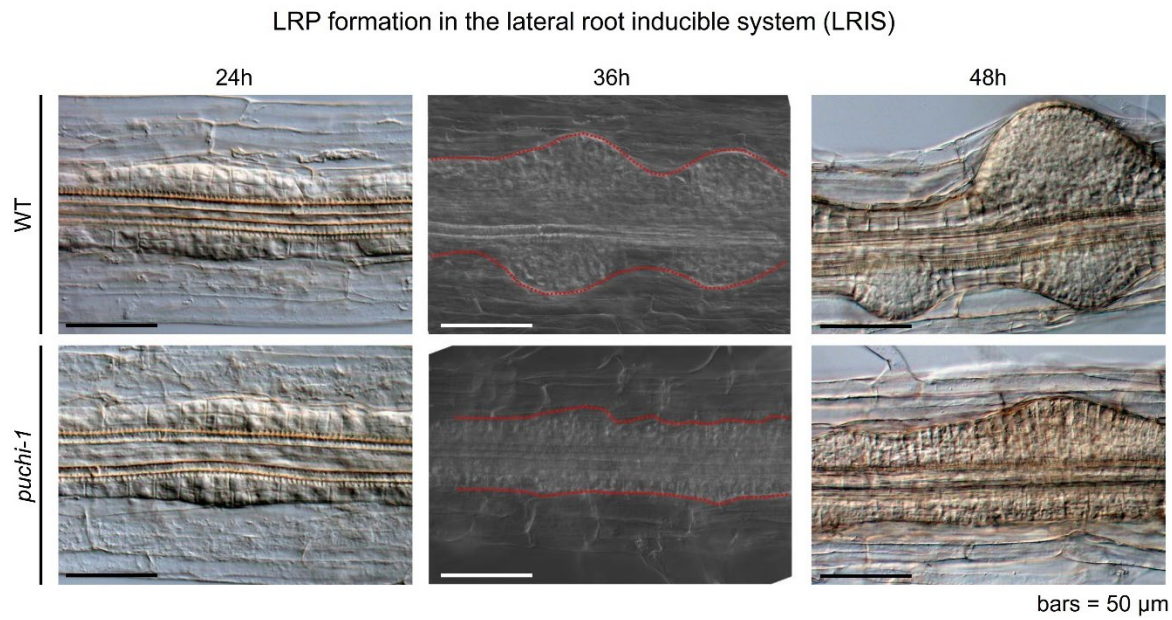

Fig. S3. LRPs in WT and *puchi-1* seedlings after incubation on the lateral root inducible system (LRIS) for indicated durations.

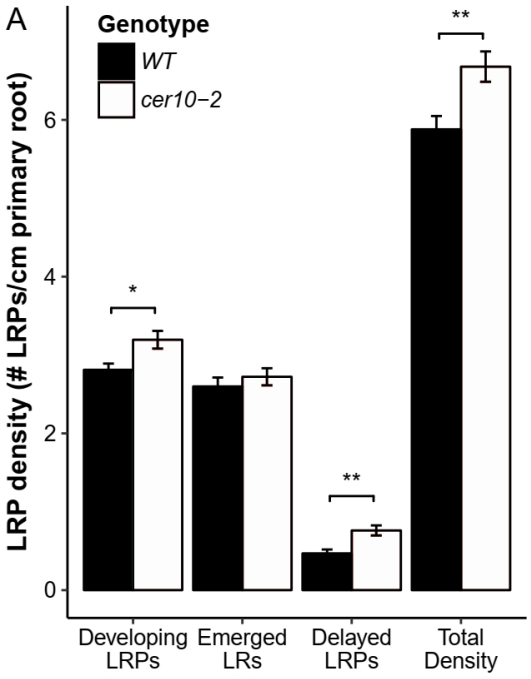

Fig. S4. Mutant in the *ECR* gene produced more lateral organs than did WT. Density of developing LRPs, emerged LRs, delayed LRPs, and total LR initiations (LRPs + LRs) in 9-day old WT and *cer10-2* seedlings. The figure is representative for 3 biological repeats which gave similar results. n ≥ 20 for each genotype each repeat. Significance was determined by Student's t test. * $p < 0.05$, ** $p < 0.01$.

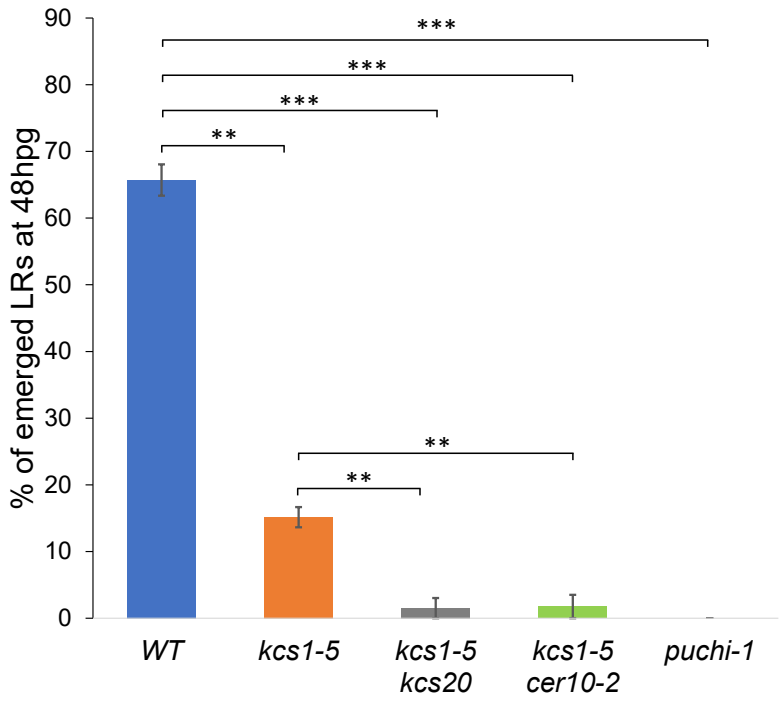

Fig. S5. Double mutants of VLCFA genes resulted in a stronger LRP emergence defect than *kcs1-5* single mutant. The percentages of emerged LRs over total LRPs at 48 hours post gravistimulation (hpg) are presented. Data are represented as Mean ± SEM of 2, 2, 3, 3 and 3 biological replicates for WT, *kcs1-5, kcs1-5 kcs20, kcs1-5 cer10-2* and *puchi-1*, respectively, with number of seedlings ≥ 20 in each repeat. At 48h after gravistimulation, none of *puchi-1* LRPs emerged. Significance was determined by Student's t test. * $p < 0.05$, ** $p < 0.01$, *** $p < 0.001$.

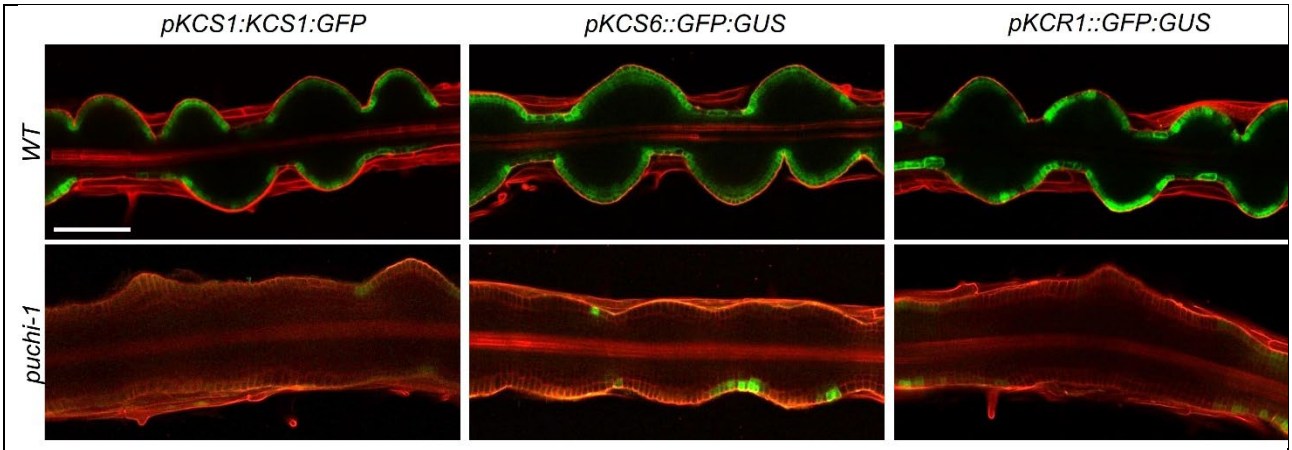

Fig. S6. PUCHI is required for the correct expression pattern of three VLCFA reporter lines (*pKCS1::KCS1:GFP, pKCS6::GFP:GUS* and *pKCR1::GFP:GUS*) in the context of callus formation. Seedlings were grown on MS/2 medium for seven days then transferred to callus inducing medium (CIM) for 4 days. Bar = 100 µm.

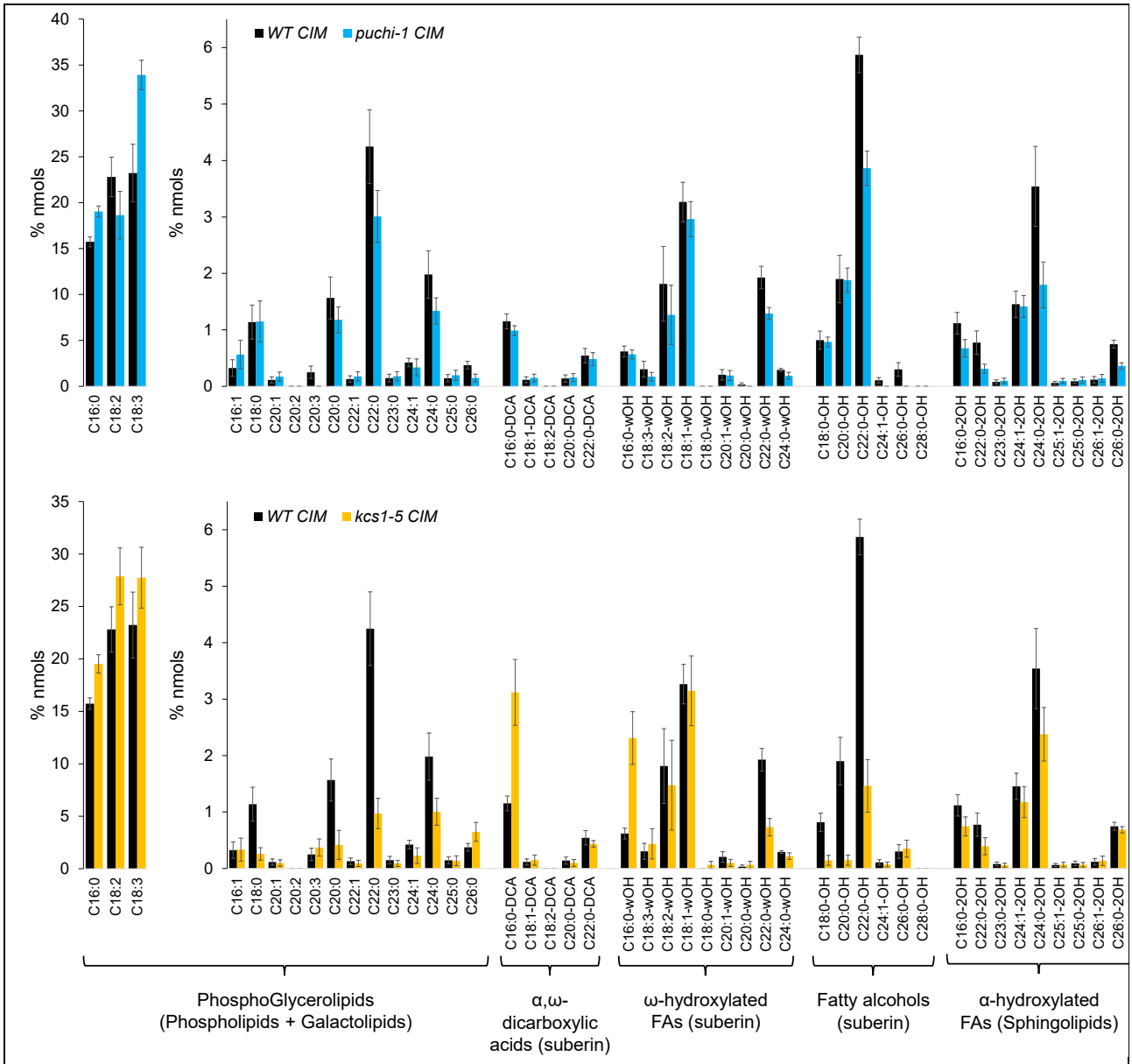

Fig. S7. Global fatty acids of WT, *puchi-1* (upper panel) and WT, *kcs1-5* (lower panel) roots after 4 days on CIM. -DCA: α,ω-dicarboxylic acid; ωOH-: ω-hydroxy acids; -OH: fatty alcohols; h-: 2-hydroxy fatty acids. The brackets indicate the typical cellular components of the corresponding FA species. For example, 22:0-OH is a fatty alcohol that is typically found in root suberin. Data are represented as Mean ± SEM of six, six and five biological replicates for WT, *puchi-1* and *kcs1-5*, respectively.

Table S1. TAIR ID and names of the 217 genes showing an expression profile similar to that of *PUCHI* as revealed by TDCor.

Gene names retrieved from TAIR:

https://www.arabidopsis.org/tools/bulk/genes/index.jsp

ID	Gene Name
AT1G01120	3-KETOACYL-COA SYNTHASE 1 (*KCS1*)
AT1G01610	GLYCEROL-3-PHOSPHATE ACYLTRANSFERASE 4 (*GPAT4*)
AT1G04040	HAD SUPERFAMILY, SUBFAMILY IIIB ACID PHOSPHATASE (AT1G04040)
AT1G04220	3-KETOACYL-COA SYNTHASE 2 (*KCS2*)
AT1G04330	HYPOTHETICAL PROTEIN (AT1G04330)
AT1G06640	2-OXOGLUTARATE (2OG) AND FE (II)-DEPENDENT OXYGENASE SUPERFAMILY PROTEIN (AT1G06640)
AT1G06650	2-OXOGLUTARATE (2OG) AND FE (II)-DEPENDENT OXYGENASE SUPERFAMILY PROTEIN (AT1G06650)
AT1G07240	UDP-GLUCOSYL TRANSFERASE 71C5 (*UGT71C5*)
AT1G08310	ALPHA/BETA-HYDROLASES SUPERFAMILY PROTEIN (AT1G08310)
AT1G08480	SUCCINATE DEHYDROGENASE SUBUNIT (*SDH6*)
AT1G09560	GERMIN-LIKE PROTEIN 5 (*GLP5*)
AT1G10730	CLATHRIN ADAPTOR COMPLEXES MEDIUM SUBUNIT FAMILY PROTEIN (AT1G10730)
AT1G13080	CYTOCHROME P450, FAMILY 71, SUBFAMILY B, POLYPEPTIDE 2 (*CYP71B2*)
AT1G14130	2-OXOGLUTARATE (2OG) AND FE (II)-DEPENDENT OXYGENASE SUPERFAMILY PROTEIN (AT1G14130)
AT1G14340	RNA-BINDING (RRM/RBD/RNP MOTIFS) FAMILY PROTEIN (AT1G14340)
AT1G17860	KUNITZ FAMILY TRYPSIN AND PROTEASE INHIBITOR PROTEIN (AT1G17860)
AT1G17980	POLY (A) POLYMERASE 1 (*PAPS1*)
AT1G18720	ER MEMBRANE PROTEIN, PUTATIVE (DUF962) (AT1G18720)
AT1G19250	FLAVIN-DEPENDENT MONOOXYGENASE 1 (*FMO1*)
AT1G23800	ALDEHYDE DEHYDROGENASE 2B7 (*ALDH2B7*)
AT1G23850	TRANSMEMBRANE PROTEIN (AT1G23850)
AT1G26590	C2H2-LIKE ZINC FINGER PROTEIN (AT1G26590)
AT1G27980	DIHYDROSPHINGOSINE PHOSPHATE LYASE (*DPL1*)
AT1G30370	ALPHA/BETA-HYDROLASES SUPERFAMILY PROTEIN (*DLAH*)

AT1G30400	MULTIDRUG RESISTANCE-ASSOCIATED PROTEIN 1 (*ABCC1*)
AT1G30500	NUCLEAR FACTOR Y, SUBUNIT A7 (*NF-YA7*)
AT1G31940	CYSTIC FIBROSIS TRANSMEMBRANE CONDUCTANCE REGULATOR (AT1G31940)
AT1G33090	MATE EFFLUX FAMILY PROTEIN (AT1G33090)
AT1G33100	MATE EFFLUX FAMILY PROTEIN (AT1G33100)
AT1G33490	E3 UBIQUITIN-PROTEIN LIGASE (AT1G33490)
AT1G34340	ALPHA/BETA-HYDROLASES SUPERFAMILY PROTEIN (AT1G34340)
AT1G35560	TCP FAMILY TRANSCRIPTION FACTOR (AT1G35560)
AT1G48300	DIACYLGLYCEROL ACYLTRANSFERASE (*DGAT3*)
AT1G48600	S-ADENOSYL-L-METHIONINE-DEPENDENT METHYLTRANSFERASES SUPERFAMILY PROTEIN (*PMEAMT*)
AT1G48750	BIFUNCTIONAL INHIBITOR/LIPID-TRANSFER PROTEIN/SEED STORAGE 2S ALBUMIN SUPERFAMILY PROTEIN (AT1G48750)
AT1G52420	UDP-GLYCOSYLTRANSFERASE SUPERFAMILY PROTEIN (AT1G52420)
AT1G53270	ABC-2 TYPE TRANSPORTER FAMILY PROTEIN (*ABCG10*)
AT1G53280	CLASS I GLUTAMINE AMIDOTRANSFERASE-LIKE SUPERFAMILY PROTEIN (*DJ1B*)
AT1G54920	HYPOTHETICAL PROTEIN (AT1G54920)
AT1G55960	POLYKETIDE CYCLASE/DEHYDRASE AND LIPID TRANSPORT SUPERFAMILY PROTEIN (AT1G55960)
AT1G56500	HALOACID DEHALOGENASE-LIKE HYDROLASE FAMILY PROTEIN (AT1G56500)
AT1G63440	HEAVY METAL ATPASE 5 (*HMA5*)
AT1G64780	AMMONIUM TRANSPORTER 1;2 (*AMT1;2*)
AT1G64860	SIGMA FACTOR A (*SIGA*)
AT1G65820	MICROSOMAL GLUTATHIONE S-TRANSFERASE (AT1G65820)
AT1G65850	DISEASE RESISTANCE PROTEIN (TIR-NBS-LRR CLASS) FAMILY (AT1G65850)
AT1G66240	HOMOLOG OF ANTI-OXIDANT 1 (*ATX1*)
AT1G67730	BETA-KETOACYL REDUCTASE 1 (*KCR1*)
AT1G68300	ADENINE NUCLEOTIDE ALPHA HYDROLASES-LIKE SUPERFAMILY PROTEIN (AT1G68300)
AT1G69850	NITRATE TRANSPORTER 1:2 (*NRT1:2*)
AT1G70470	TRANSMEMBRANE PROTEIN (AT1G70470)
AT1G72540	PROTEIN KINASE SUPERFAMILY PROTEIN (AT1G72540)

AT1G72800	RNA-BINDING (RRM/RBD/RNP MOTIFS) FAMILY PROTEIN (AT1G72800)
AT1G73500	MAP KINASE KINASE 9 (*MKK9*)
AT1G74210	PLC-LIKE PHOSPHODIESTERASES SUPERFAMILY PROTEIN (GDPD5)
AT1G74770	ZINC ION BINDING PROTEIN (AT1G74770)
AT1G75370	SEC14P-LIKE PHOSPHATIDYLINOSITOL TRANSFER FAMILY PROTEIN (AT1G75370)
AT1G75920	GDSL-LIKE LIPASE/ACYLHYDROLASE SUPERFAMILY PROTEIN (AT1G75920)
AT1G76150	ENOYL-COA HYDRATASE 2 (*ECH2*)
AT1G76360	PROTEIN KINASE SUPERFAMILY PROTEIN (AT1G76360)
AT1G77420	ALPHA/BETA-HYDROLASES SUPERFAMILY PROTEIN (AT1G77420)
AT1G77600	ARM REPEAT SUPERFAMILY PROTEIN (AT1G77600)
AT1G78320	GLUTATHIONE S-TRANSFERASE TAU 23 (*GSTU23*)
AT1G79700	INTEGRASE-TYPE DNA-BINDING SUPERFAMILY PROTEIN (*WRI4*)
AT2G11520	CALMODULIN-BINDING RECEPTOR-LIKE CYTOPLASMIC KINASE 3 (*CRCK3*)
AT2G17430	SEVEN TRANSMEMBRANE MLO FAMILY PROTEIN (*MLO7*)
AT2G17500	AUXIN EFFLUX CARRIER FAMILY PROTEIN (AT2G17500)
AT2G17640	TRIMERIC LPXA-LIKE ENZYMES SUPERFAMILY PROTEIN (*ATSERAT3;1*)
AT2G17650	AMP-DEPENDENT SYNTHETASE AND LIGASE FAMILY PROTEIN (AT2G17650)
AT2G18490	C2H2-LIKE ZINC FINGER PROTEIN (AT2G18490)
AT2G22660	DNA-BINDING PROTEIN, PUTATIVE (DUPLICATED DUF1399) (AT2G22660)
AT2G23320	WRKY DNA-BINDING PROTEIN 15 (*WRKY15*)
AT2G27550	CENTRORADIALI (ATC)
AT2G32560	F-BOX FAMILY PROTEIN (AT2G32560)
AT2G33330	PLASMODESMATA-LOCATED PROTEIN 3 (*PDLP3*)
AT2G35060	K+ UPTAKE PERMEASE 11 (*KUP11*)
AT2G35780	SERINE CARBOXYPEPTIDASE-LIKE 26 (*SCPL26*)
AT2G37460	NODULIN MTN21 /EAMA-LIKE TRANSPORTER FAMILY PROTEIN (*UMAMIT12*)
AT2G37760	NAD (P)-LINKED OXIDOREDUCTASE SUPERFAMILY PROTEIN (*AKR4C8*)
AT2G38460	IRON REGULATED 1 (*IREG1*)
AT2G41120	DUF309 DOMAIN PROTEIN (AT2G41120)
AT2G41480	PEROXIDASE SUPERFAMILY PROTEIN (AT2G41480)

AT2G42600	PHOSPHOENOLPYRUVATE CARBOXYLASE 2 (*PPC2*)
AT2G42790	CITRATE SYNTHASE 3 (*CSY3*)
AT2G43320	S-ADENOSYL-L-METHIONINE-DEPENDENT METHYLTRANSFERASES SUPERFAMILY PROTEIN (AT2G43320)
AT2G43420	3-BETA HYDROXYSTEROID DEHYDROGENASE/ISOMERASE FAMILY PROTEIN (AT2G43420)
AT2G43680	IQ-DOMAIN 14 (*IQD14*)
AT2G44230	HYPOTHETICAL PROTEIN (*DUF946*) (AT2G44230)
AT2G46100	NUCLEAR TRANSPORT FACTOR 2 (*NTF2*) FAMILY PROTEIN (AT2G46100)
AT2G47630	ALPHA/BETA-HYDROLASES SUPERFAMILY PROTEIN (AT2G47630)
AT2G48130	BIFUNCTIONAL INHIBITOR/LIPID-TRANSFER PROTEIN/SEED STORAGE 2S ALBUMIN SUPERFAMILY PROTEIN (AT2G48130)
AT2G48140	BIFUNCTIONAL INHIBITOR/LIPID-TRANSFER PROTEIN/SEED STORAGE 2S ALBUMIN SUPERFAMILY PROTEIN (*EDA4*)
AT3G01210	RNA-BINDING (RRM/RBD/RNP MOTIFS) FAMILY PROTEIN (AT3G01210)
AT3G01690	ALPHA/BETA-HYDROLASES SUPERFAMILY PROTEIN (AT3G01690)
AT3G01930	MAJOR FACILITATOR SUPERFAMILY PROTEIN (AT3G01930)
AT3G02730	THIOREDOXIN F-TYPE 1 (*TRXF1*)
AT3G03490	PEROXIN 19-1 (*PEX19-1*)
AT3G06510	GLYCOSYL HYDROLASE SUPERFAMILY PROTEIN (*SFR2*)
AT3G07130	PURPLE ACID PHOSPHATASE 15 (*PAP15*)
AT3G07720	GALACTOSE OXIDASE/KELCH REPEAT SUPERFAMILY PROTEIN (AT3G07720)
AT3G08510	PHOSPHOLIPASE C 2 (*PLC2*)
AT3G11080	RECEPTOR LIKE PROTEIN 35 (*RLP35*)
AT3G13090	MULTIDRUG RESISTANCE-ASSOCIATED PROTEIN 8 (*ABCC6*)
AT3G13790	GLYCOSYL HYDROLASES FAMILY 32 PROTEIN (*ATBFRUCT1*)
AT3G14570	GLUCAN SYNTHASE-LIKE 4 (*GSL04*)
AT3G15760	CYTOCHROME P450 FAMILY PROTEIN (AT3G15760)
AT3G20120	CYTOCHROME P450, FAMILY 705, SUBFAMILY A, POLYPEPTIDE 21 (*CYP705A21*)
AT3G21260	GLYCOLIPID TRANSFER PROTEIN (GLTP) FAMILY PROTEIN (*GLTP3*)
AT3G22160	VQ MOTIF-CONTAINING PROTEIN (AT3G22160)
AT3G23430	PHOSPHATE 1 (*PHO1*)
AT3G23600	ALPHA/BETA-HYDROLASES SUPERFAMILY PROTEIN (AT3G23600)

AT3G25610	ATPASE E1-E2 TYPE FAMILY PROTEIN / HALOACID DEHALOGENASE-LIKE HYDROLASE FAMILY PROTEIN (AT3G25610)
AT3G26830	CYTOCHROME P450 SUPERFAMILY PROTEIN (*PAD3*)
AT3G27090	DCD (DEVELOPMENT AND CELL DEATH) DOMAIN PROTEIN (AT3G27090)
AT3G44990	XYLOGLUCAN ENDO-TRANSGLYCOSYLASE-RELATED 8 (*XTH31*)
AT3G45410	CONCANAVALIN A-LIKE LECTIN PROTEIN KINASE FAMILY PROTEIN (AT3G45410)
AT3G45640	MITOGEN-ACTIVATED PROTEIN KINASE 3 (*MPK3*)
AT3G50350	MEMBRANE INSERTASE, PUTATIVE (DUF1685) (AT3G50350)
AT3G51430	CALCIUM-DEPENDENT PHOSPHOTRIESTERASE SUPERFAMILY PROTEIN (*YLS2*)
AT3G51520	DIACYLGLYCEROL ACYLTRANSFERASE FAMILY (*DGAT2*)
AT3G52850	VACUOLAR SORTING RECEPTOR HOMOLOG 1 (*VSR1*)
AT3G53820	C2H2 AND C2HC ZINC FINGERS SUPERFAMILY PROTEIN (AT3G53820)
AT3G54010	FKBP-TYPE PEPTIDYL-PROLYL CIS-TRANS ISOMERASE FAMILY PROTEIN (*PAS1*)
AT3G54420	HOMOLOG OF CARROT EP3-3 CHITINASE (*EP3*)
AT3G55090	ABC-2 TYPE TRANSPORTER FAMILY PROTEIN (*ABCG16*)
AT3G56360	HYPOTHETICAL PROTEIN (AT3G56360)
AT3G56730	PUTATIVE ENDONUCLEASE OR GLYCOSYL HYDROLASE (AT3G56730)
AT3G56980	BASIC HELIX-LOOP-HELIX (BHLH) DNA-BINDING SUPERFAMILY PROTEIN (*BHLH39*)
AT3G58170	BET1P/SFT1P-LIKE PROTEIN 14A (*BS14A*)
AT3G61200	THIOESTERASE SUPERFAMILY PROTEIN (AT3G61200)
AT3G62560	RAS-RELATED SMALL GTP-BINDING FAMILY PROTEIN (AT3G62560)
AT3G63170	CHALCONE-FLAVANONE ISOMERASE FAMILY PROTEIN (*FAP1*)
AT4G00030	PLASTID-LIPID ASSOCIATED PROTEIN PAP / FIBRILLIN FAMILY PROTEIN (AT4G00030)
AT4G00880	SAUR-LIKE AUXIN-RESPONSIVE PROTEIN FAMILY (AT4G00880)
AT4G01440	NODULIN MTN21 /EAMA-LIKE TRANSPORTER FAMILY PROTEIN (UMAMIT31)
AT4G01610	CYSTEINE PROTEINASES SUPERFAMILY PROTEIN (AT4G01610)
AT4G03260	OUTER ARM DYNEIN LIGHT CHAIN 1 PROTEIN (AT4G03260)
AT4G03960	PHOSPHOTYROSINE PROTEIN PHOSPHATASES SUPERFAMILY PROTEIN (*PFA-DSP4*)

AT4G04470	PEROXISOMAL MEMBRANE 22 KDA (MPV17/PMP22) FAMILY PROTEIN (*PMP22*)
AT4G04830	METHIONINE SULFOXIDE REDUCTASE B5 (*MSRB5*)
AT4G11960	PGR5-LIKE B (*PGRL1B*)
AT4G12390	PECTIN METHYLESTERASE INHIBITOR 1 (*PME1*)
AT4G14710	RMLC-LIKE CUPINS SUPERFAMILY PROTEIN (*ATARD2*)
AT4G18360	ALDOLASE-TYPE TIM BARREL FAMILY PROTEIN (*GOX3*)
AT4G18880	HEAT SHOCK TRANSCRIPTION FACTOR A4A (*HSF A4A*)
AT4G20000	VQ MOTIF-CONTAINING PROTEIN (AT4G20000)
AT4G21910	MATE EFFLUX FAMILY PROTEIN (AT4G21910)
AT4G22890	PGR5-LIKE A (*PGR5-LIKE A*)
AT4G23880	HYPOTHETICAL PROTEIN (AT4G23880)
AT4G23980	AUXIN RESPONSE FACTOR 9 (*ARF9*)
AT4G24130	DUF538 FAMILY PROTEIN (PROTEIN OF UNKNOWN FUNCTION, DUF538) (AT4G24130)
AT4G27710	CYTOCHROME P450, FAMILY 709, SUBFAMILY B, POLYPEPTIDE 3 (*CYP709B3*)
AT4G28110	MYB DOMAIN PROTEIN 41 (*MYB41*)
AT4G30830	MYOSIN-LIKE PROTEIN (PROTEIN OF UNKNOWN FUNCTION, DUF593) (AT4G30830)
AT4G31240	PROTEIN KINASE C-LIKE ZINC FINGER PROTEIN (AT4G31240)
AT4G31330	TRANSMEMBRANE PROTEIN, PUTATIVE (PROTEIN OF UNKNOWN FUNCTION, DUF599) (AT4G31330)
AT4G31670	UBIQUITIN-SPECIFIC PROTEASE 18 (*UBP18*)
AT4G32650	POTASSIUM CHANNEL PROTEIN (*KAT3*)
AT4G33160	F-BOX FAMILY PROTEIN (AT4G33160)
AT4G33420	PEROXIDASE SUPERFAMILY PROTEIN (AT4G33420)
AT4G34120	CYSTATHIONINE BETA-SYNTHASE (CBS) FAMILY PROTEIN (*LEJ1*)
AT4G35220	CYCLASE FAMILY PROTEIN (AT4G35220)
AT4G36140	DISEASE RESISTANCE PROTEIN (TIR-NBS-LRR CLASS) (AT4G36140)
AT4G36610	ALPHA/BETA-HYDROLASES SUPERFAMILY PROTEIN (AT4G36610)
AT4G37200	THIOREDOXIN SUPERFAMILY PROTEIN (*HCF164*)
AT5G02100	OXYSTEROL-BINDING FAMILY PROTEIN (*UNE18*)
AT5G02560	HISTONE H2A 12 (*HTA12*)
AT5G02620	ANKYRIN-LIKE1 (*ANK1*)
AT5G03880	THIOREDOXIN FAMILY PROTEIN (AT5G03880)

AT5G04150	BASIC HELIX-LOOP-HELIX (BHLH) DNA-BINDING SUPERFAMILY PROTEIN (BHLH101)
AT5G05250	HYPOTHETICAL PROTEIN (AT5G05250)
AT5G06960	OCS-ELEMENT BINDING FACTOR 5 (*OBF5*)
AT5G08240	TRANSMEMBRANE PROTEIN (AT5G08240)
AT5G08500	TRANSMEMBRANE CLPTM1 FAMILY PROTEIN (AT5G08500)
AT5G10230	ANNEXIN 7 (*ANNAT7*)
AT5G10480	PROTEIN-TYROSINE PHOSPHATASE-LIKE, PTPLA (*PAS2*)
AT5G11650	ALPHA/BETA-HYDROLASES SUPERFAMILY PROTEIN (AT5G11650)
AT5G11770	NADH-UBIQUINONE OXIDOREDUCTASE 20 KDA SUBUNIT (AT5G11770)
AT5G12420	O-ACYLTRANSFERASE (WSD1-LIKE) FAMILY PROTEIN (AT5G12420)
AT5G15240	TRANSMEMBRANE AMINO ACID TRANSPORTER FAMILY PROTEIN (AT5G15240)
AT5G17000	ZINC-BINDING DEHYDROGENASE FAMILY PROTEIN (AT5G17000)
AT5G20270	HEPTAHELICAL TRANSMEMBRANE PROTEIN1 (*HHP1*)
AT5G23840	MD-2-RELATED LIPID RECOGNITION DOMAIN-CONTAINING PROTEIN (AT5G23840)
AT5G25830	GATA TRANSCRIPTION FACTOR 12 (*GATA12*)
AT5G27350	MAJOR FACILITATOR SUPERFAMILY PROTEIN (*SFP1*)
AT5G38280	PR5-LIKE RECEPTOR KINASE (*PR5K*)
AT5G39090	HXXXD-TYPE ACYL-TRANSFERASE FAMILY PROTEIN (AT5G39090)
AT5G39610	NAC DOMAIN CONTAINING PROTEIN 6 (*NAC6*)
AT5G39730	AIG2-LIKE (AVIRULENCE INDUCED GENE) FAMILY PROTEIN (AT5G39730)
AT5G39950	THIOREDOXIN 2 (*TRX2*)
AT5G42440	PROTEIN KINASE SUPERFAMILY PROTEIN (AT5G42440)
AT5G42890	STEROL CARRIER PROTEIN 2 (*SCP2*)
AT5G42980	THIOREDOXIN 3 (*TRX3*)
AT5G45060	DISEASE RESISTANCE PROTEIN (TIR-NBS-LRR CLASS) FAMILY (AT5G45060)
AT5G46780	VQ MOTIF-CONTAINING PROTEIN (AT5G46780)
AT5G46790	PYR1-LIKE 1 (*PYL1*)
AT5G49170	HYPOTHETICAL PROTEIN (AT5G49170)
AT5G50200	NITRATE TRANSMEMBRANE TRANSPORTER (*WR3*)
AT5G50820	NAC DOMAIN CONTAINING PROTEIN 97 (*NAC097*)
AT5G51550	EXORDIUM LIKE 3 (*EXL3*)

AT5G52240	MEMBRANE STEROID BINDING PROTEIN 1 (*MSBP1*)
AT5G53110	RING/U-BOX SUPERFAMILY PROTEIN (AT5G53110)
AT5G53850	HALOACID DEHALOGENASE-LIKE HYDROLASE FAMILY PROTEIN (AT5G53850)
AT5G55970	RING/U-BOX SUPERFAMILY PROTEIN (AT5G55970)
AT5G56150	UBIQUITIN-CONJUGATING ENZYME 30 (*UBC30*)
AT5G56460	PROTEIN KINASE SUPERFAMILY PROTEIN (AT5G56460)
AT5G57390	AINTEGUMENTA-LIKE 5 (*AIL5*)
AT5G58330	LACTATE/MALATE DEHYDROGENASE FAMILY PROTEIN (AT5G58330)
AT5G59250	MAJOR FACILITATOR SUPERFAMILY PROTEIN (AT5G59250)
AT5G59590	UDP-GLUCOSYL TRANSFERASE 76E2 (*UGT76E2*)
AT5G60360	ALEURAIN-LIKE PROTEASE (*ALP*)
AT5G60900	RECEPTOR-LIKE PROTEIN KINASE 1 (*RLK1*)
AT5G62480	GLUTATHIONE S-TRANSFERASE TAU 9 (*GSTU9*)
AT5G64120	PEROXIDASE SUPERFAMILY PROTEIN (AT5G64120)
AT5G64280	DICARBOXYLATE TRANSPORTER 2.2 (*DIT2.2*)
AT5G65970	SEVEN TRANSMEMBRANE MLO FAMILY PROTEIN (*MLO10*)
ATCG00490	RIBULOSE BISPHOSPHATE CARBOXYLASE LARGE CHAIN (*RBCL*)

Table S2. Gene ontology (GO) enrichment analysis using BiNGO on the list of 217 genes downstream of *PUCHI*.

For each functional category (GO-ID), the BiNGO (3) analysis presents n = number of genes belonging to that category in the *A. thaliana* GO reference; N = number of genes in the *A. thaliana* GO reference; x = number of genes of the corresponding GO category in the studied gene list; and X = number of genes in the studied gene list for which a GO annotation is available.

Parameter of the analysis:

Selected statistical test: Hypergeometric test

Selected correction: Benjamini & Hochberg False Discovery Rate (FDR) correction

Selected significance level: 0.05

Testing option: Use whole annotation as reference set

No annotations were retrieved for the following entities:

AT1G65820; AT3G56730; AT3G01690; AT5G39090; AT1G14340; AT1G04040; AT3G01930; AT1G33100

GO-ID	p-value	corr p-value	x	n	X	N	Description
55114	2.36E-09	2.38E-06	34	1436	193	25717	oxidation-reduction process
6629	2.42E-08	1.22E-05	26	980	193	25717	lipid metabolic process
50896	4.57E-07	1.53E-04	78	6232	193	25717	response to stimulus
44281	2.08E-06	5.22E-04	30	1564	193	25717	small molecule metabolic process
6950	4.47E-06	9.00E-04	50	3520	193	25717	response to stress
43436	6.43E-06	9.67E-04	23	1075	193	25717	oxoacid metabolic process
6082	6.73E-06	9.67E-04	23	1078	193	25717	organic acid metabolic process
44255	8.63E-06	1.09E-03	17	648	193	25717	cellular lipid metabolic process
45454	1.06E-05	1.18E-03	8	139	193	25717	cell redox homeostasis
6631	1.26E-05	1.26E-03	10	236	193	25717	fatty acid metabolic process
42592	1.38E-05	1.26E-03	15	535	193	25717	homeostatic process
19752	2.94E-05	2.47E-03	20	941	193	25717	carboxylic acid metabolic process
6662	5.47E-05	4.23E-03	4	28	193	25717	glycerol ether metabolic process
18904	8.26E-05	5.48E-03	4	31	193	25717	ether metabolic process
52317	8.71E-05	5.48E-03	3	12	193	25717	camalexin metabolic process
10120	8.71E-05	5.48E-03	3	12	193	25717	camalexin biosynthetic process
9404	9.56E-05	5.51E-03	5	61	193	25717	toxin metabolic process
38	1.06E-04	5.51E-03	4	33	193	25717	very long-chain fatty acid metabolic process

6810	1.10E-04	5.51E-03	34	2312	193	25717	transport
51234	1.34E-04	5.51E-03	34	2336	193	25717	establishment of localization
32787	1.40E-04	5.51E-03	12	443	193	25717	monocarboxylic acid metabolic process
52314	1.43E-04	5.51E-03	3	14	193	25717	phytoalexin metabolic process
52315	1.43E-04	5.51E-03	3	14	193	25717	phytoalexin biosynthetic process
46217	1.43E-04	5.51E-03	3	14	193	25717	indole phytoalexin metabolic process
9403	1.43E-04	5.51E-03	3	14	193	25717	toxin biosynthetic process
9700	1.43E-04	5.51E-03	3	14	193	25717	indole phytoalexin biosynthetic process
42761	1.77E-04	6.60E-03	3	15	193	25717	very long-chain fatty acid biosynthetic process
42221	1.87E-04	6.61E-03	39	2883	193	25717	response to chemical
6979	1.91E-04	6.61E-03	12	458	193	25717	response to oxidative stress
51179	2.67E-04	8.95E-03	34	2423	193	25717	localization
6869	4.07E-04	1.26E-02	7	178	193	25717	lipid transport
44248	4.12E-04	1.26E-02	19	1059	193	25717	cellular catabolic process
65008	4.14E-04	1.26E-02	18	974	193	25717	regulation of biological quality
19725	4.86E-04	1.44E-02	9	302	193	25717	cellular homeostasis
6099	5.41E-04	1.50E-02	4	50	193	25717	tricarboxylic acid cycle
6101	5.41E-04	1.50E-02	4	50	193	25717	citrate metabolic process
51775	5.52E-04	1.50E-02	2	5	193	25717	response to redox state
71702	6.46E-04	1.71E-02	20	1188	193	25717	organic substance transport
72350	7.25E-04	1.87E-02	4	54	193	25717	tricarboxylic acid metabolic process
10106	8.24E-04	2.07E-02	2	6	193	25717	cellular response to iron ion starvation
10876	8.87E-04	2.18E-02	7	203	193	25717	lipid localization
45926	1.32E-03	3.14E-02	3	29	193	25717	negative regulation of growth
45088	1.35E-03	3.14E-02	5	108	193	25717	regulation of innate immune response
9056	1.39E-03	3.14E-02	22	1453	193	25717	catabolic process
9636	1.41E-03	3.14E-02	5	109	193	25717	response to toxic substance
9060	1.46E-03	3.17E-02	4	65	193	25717	aerobic respiration
44272	1.48E-03	3.17E-02	6	163	193	25717	sulfur compound biosynthetic process
50776	1.65E-03	3.46E-02	5	113	193	25717	regulation of immune response
44242	1.82E-03	3.73E-02	4	69	193	25717	cellular lipid catabolic process
6635	1.92E-03	3.77E-02	3	33	193	25717	fatty acid beta-oxidation
8152	1.94E-03	3.77E-02	103	11008	193	25717	metabolic process

19509	1.95E-03	3.77E-02	2	9	193	25717	L-methionine salvage from methylthioadenosine
6790	2.08E-03	3.84E-02	9	372	193	25717	sulfur compound metabolic process
9062	2.10E-03	3.84E-02	3	34	193	25717	fatty acid catabolic process
42335	2.10E-03	3.84E-02	3	34	193	25717	cuticle development
8610	2.38E-03	4.16E-02	11	532	193	25717	lipid biosynthetic process
43102	2.42E-03	4.16E-02	2	10	193	25717	amino acid salvage
71267	2.42E-03	4.16E-02	2	10	193	25717	L-methionine salvage
9607	2.44E-03	4.16E-02	20	1328	193	25717	response to biotic stimulus
2682	2.56E-03	4.20E-02	5	125	193	25717	regulation of immune system process
6811	2.59E-03	4.20E-02	13	702	193	25717	ion transport
9624	2.59E-03	4.20E-02	4	76	193	25717	response to nematode
19395	2.68E-03	4.28E-02	3	37	193	25717	fatty acid oxidation
9628	2.74E-03	4.30E-02	27	2036	193	25717	response to abiotic stimulus
6970	2.99E-03	4.63E-02	12	630	193	25717	response to osmotic stress
45333	3.04E-03	4.63E-02	5	130	193	25717	cellular respiration
19748	3.37E-03	4.92E-02	10	477	193	25717	secondary metabolic process
10497	3.52E-03	4.92E-02	2	12	193	25717	plasmodesmata-mediated intercellular transport
9819	3.52E-03	4.92E-02	2	12	193	25717	drought recovery
71265	3.52E-03	4.92E-02	2	12	193	25717	L-methionine biosynthetic process
30497	3.52E-03	4.92E-02	2	12	193	25717	fatty acid elongation
10204	3.52E-03	4.92E-02	2	12	193	25717	defense response signaling pathway, resistance gene-independent

Table S3

Genes in *pPUCHI::PUCHI:GR* in *puchi-1* seedlings showed an upregulation (fold change ≥ 1.5, *p-value* ≤ 0.05) in two treatment combinations: NAA + DEX versus NAA, and NAA + DEX + CHX versus NAA + DEX

(GR: GLUCOCORTICOID RECEPTOR; DEX: dexamethasone; CHX: cycloheximide)

NAA DEX vs NAA: 48 genes, 1 VLCFA gene (*KCS8*)

Gene ID	Common name	Fold change	*p_value* (Welch Two Sample t-test)
AT1G01600	CYTOCHROME P450, FAMILY 86, SUBFAMILY A, POLYPEPTIDE 4 (CYP86A4)	1.5	0.02
AT1G03700	CASP-LIKE PROTEIN 1C2 (CASPL1C2)	1.5	0.04
AT1G16310		1.6	0.03
AT1G18690	XYLOGLUCAN XYLOSYLTRANSFERASE 4 (XXT4)	1.5	0.04
AT1G28360	ERF DOMAIN PROTEIN 12 (ERF12)	1.7	0.04
AT1G29195		1.5	0.03
AT1G30860		1.6	0.03
AT1G35140	PHOSPHATE-INDUCED 1 (PHI-1)	1.5	0.01
AT1G61260		1.6	0.02
AT1G64700		1.8	0.03
AT1G70470		1.9	0.02
AT1G75900		1.7	0.01
AT2G15090	3-KETOACYL-COA SYNTHASE 8 (KCS8)	1.8	0.00
AT2G16630	FUSED OUTER CUTICULAR LEDGE1 (FOCL1)	1.7	0.03
AT2G28950	EXPANSIN A6 (EXPA6)	1.6	0.01
AT2G42430	LATERAL ORGAN BOUNDARIES-DOMAIN 16 (LBD16)	1.8	0.01
AT2G44260		1.5	0.03
AT2G46990	INDOLE-3-ACETIC ACID INDUCIBLE 20 (IAA20)	1.7	0.02
AT3G05470	FORMIN 11 (FH11)	1.8	0.01
AT3G52920		1.5	0.04
AT3G56060		1.6	0.03
AT4G03620		1.5	0.03

AT4G08780		2.6	0.03
AT4G11140	CYTOKININ RESPONSE FACTOR 1 (CRF1)	3.1	0.01
AT4G14330		1.5	0.02
AT4G14750	IQ-DOMAIN 19 (IQD19)	1.5	0.03
AT4G19980		1.5	0.01
AT4G28430	RETICULON 18 (RTN18)	1.8	0.01
AT4G29080	PHYTOCHROME-ASSOCIATED PROTEIN 2 (PAP2)	1.7	0.03
AT4G36260	STYLISH 2 (STY2)	2.1	0.01
AT4G37490	CYCLIN B1;1 (CYCB1;1)	1.6	0.03
AT4G37580	HOOKLESS 1 (HLS1)	1.5	0.02
AT4G38770	PROLINE-RICH PROTEIN 4 (PRP4)	1.9	0.03
AT5G02540		1.6	0.05
AT5G09800		1.6	0.01
AT5G17160		1.6	0.01
AT5G23940	PERMEABLE LEAVES3 (PEL3)	1.5	0.03
AT5G24600		1.5	0.01
AT5G24910	CYTOCHROME P450, FAMILY 714, SUBFAMILY A, POLYPEPTIDE 1 (CYP714A1)	1.6	0.02
AT5G45670		2.7	0.01
AT5G45700		1.6	0.01
AT5G50120		1.6	0.01
AT5G51550	EXORDIUM LIKE 3 (EXL3)	1.6	0.03
AT5G54130		1.5	0.01
AT5G62470	MYB DOMAIN PROTEIN 96 (MYB96)	1.7	0.03
AT5G66440	CYTOCHROME P450, FAMILY 86, SUBFAMILY A, POLYPEPTIDE 4 (CYP86A4)	1.5	0.05

Table S3 (cont.)

Genes in *pPUCHI::PUCHI:GR* in *puchi-1* seedlings showed an upregulation (fold change ≥ 1.5, *p-value* ≤ 0.05) in two conditions: NAA + DEX and NAA + DEX + CHX

NAA CHX DEX vs NAA CHX: 13 genes, 0 VLCFA gene

Gene ID	Common name	Fold change	*p_value* (Welch Two Sample t-test)
AT1G80590	WRKY DNA-BINDING PROTEIN 66 (WRKY66)	2.7	0.02
AT3G17150		2.1	0.03
AT3G49380	IQ-DOMAIN 15 (IQD15)	1.5	0.02
AT3G50310	MITOGEN-ACTIVATED PROTEIN KINASE KINASE KINASE 20 (MAPKKK20)	1.5	0.02
AT3G53960		1.6	0.04
AT3G55720	BOUNDARY OF ROP DOMAIN7 (BDR7)	2.5	0.03
AT3G57950		2.2	0.04
AT4G11140	CYTOKININ RESPONSE FACTOR 1 (CRF1)	3.4	0.04
AT4G14280		1.5	0.03
AT4G32540	YUCCA 1 (YUC1)	1.7	0.04
AT4G36260	STYLISH 2 (STY2)	1.7	0.02
AT5G06270		1.6	0.05
AT5G06870	POLYGALACTURONASE INHIBITING PROTEIN 2 (PGIP2)	1.5	0.03

Table S4. Tracking the numbers of emerged LRs in the branching zone after 4 and 9 days of further growth (2 separate experiments)

Time points	No. of emerged LRs at T0 (9d old plants)	No. of emerged LRs at T0 + 4d	% increase
WT	234	235	0.4
puchi-1	139	141	1.4

Table S5. Primers for qPCR used in this study.

No.	Primer name	Primer sequence (5' – 3')
1	CDKA F	ATTGCGTATTGCCACTCTCATAGG
	CDKA R	TCCTGACAGGGATACCGAATGC
2	ECR F	CCTTGACCTCCCCGATTC
	ECR R	CCAGGAGTCACGGGAAGA
3	KCS1 F	CTTGCAACGTGACCACCAT
	KCS1 R	AGCACGGTTCCGGTTAAAG
4	KCS2 F	CCATTGATCTCGCTAAACAGC
	KCS2 R	TCGGTCGTTGCCTAAATACC
5	KCS20 F	GCTTAGAGGCAACATTTTGAGC
	KCS20 R	GCGTATGAGTTTGGTTGCAC
6	KCR1 F	GCTTAAGAGGAAGAAAGGTGCTATT
	KCR R	CACTTTGTGAACTGATCCACGTA
7	PAS2 F	TCTATGACGCCATTGAGAAGC
	PAS2 R	CAGGAGATCTGACCAAACCTACTAA

References

1. Lavenus J, et al. (2015) Inference of the Arabidopsis Lateral Root Gene Regulatory Network Suggests a Bifurcation Mechanism That Defines Primordia Flanking and Central Zones. *Plant Cell* 27(5):1368–1388.
2. Voß U, et al. (2015) The circadian clock rephases during lateral root organ initiation in Arabidopsis thaliana. *Nat Commun* 6(May):7641.
3. Maere S, Heymans K, Kuiper M (2005) BiNGO: A Cytoscape plugin to assess overrepresentation of Gene Ontology categories in Biological Networks. *Bioinformatics* 21(16):3448–3449.